Zeitschrift für Geomorphologie, Vol. 62 (2019), Suppl. 2, 001–038 **PrePub**
published in print June 2019

Extreme wave events recorded in sedimentary archives of the Geropotamos River (north-central Crete, Greece)

Vera Werner, Kalliopi Baika, Anastasia Tzigounaki, Klaus Reicherter, Ioannis Papanikolaou, Kurt Emde, Peter Fischer, Andreas Vött

With 16 figures and 2 tables

Abstract. Recent tsunami events have shown that tsunamis may propagate far inland by entering rivers mouths and may cause massive damage along the river banks. However, so far, only a few studies have been conducted such a search for studying tsunami signals in incised valley systems along the Mediterranean coasts although the tsunami hazard is high. The island of Crete is known to have been affected several times by strong tsunamis, e.g., by the AD 365 and the Late Bronze Age (LBA) Santorini tsunamis. The narrow Geropotamos River valley, distinctly incised into local bedrock and located at the northern coast of Crete and fully exposed to the Cretan Sea, was selected as a promising natural setting to search for palaeotsunami signatures in fluvial sedimentary archives. Based on a multi-electrode geoelectrical survey and a set of sediment cores, we investigated the event-geochronostratigraphic record of both the Geropotamos River mouth area and the river valley ca. 1 km upstream by means of sedimentological, geochemical, geochronological, geomorphological, and micropalaeontological methods. The sedimentary environment towards the present-day river mouth is dominated by (fluvio-)lagoonal muds since the mid-Holocene. These lagoonal sediments are intersected by six coarse-grained sand layers each representing an extreme wave event (EWE). EWE layers are up to several decimetres thick and are characterized by an allochthonous foraminiferal assemblage comprising shallow marine to open marine species. Also ca. 1 km further upstream, the sedimentary record revealed grain size and microfossil evidence of two high-energy events showing a clear marine imprint. Based on this, we suggest inundation from the seaside that reached minimum 1 km inland and left EWE signatures in a presently inactive external bank position of the Geropotamos River. Considering the sedimentary characteristics, the local wind and wave climate of the Cretan Sea, and the overall geomorphological setting, we interpret these EWE layers as tsunami-related.

A major hiatus identified in the Geropotamos River mouth sediments seems to be related to the LBA Santorini tsunami as can be inferred based on local age-depth relations. The LBA tsunami is known to have severely hit the northern coast of Crete. However, the hiatus may also reflect changes in the subsidence rate and the local accommodation space architecture. The youngest EWE signal in the Geropotamos River archive appears to have been caused by the AD 365 tsunami event. Candidate deposits for both tsunami deposits were identified ca. 1 km further inland. Evidence of EWE impact documents channelling and acceleration effects of intruding water masses caused by the narrow and steeply incised Geropotamos River valley in an upstream direction. Further geochronological studies based on OSL dating are necessary for a reliable age control of these EWE candidate layers.

Keywords: palaeotsunami, incised valley systems, palaeogeography, geoarchive, coseismic uplift, multi-proxy, Crete

www.borntraeger-cramer.de
DOI: 10.1127/zfg_suppl/2019/0602 0372-8854/19/0602 $ 9.50

1 *Introduction*

The Greek island of Crete has been affected by numerous major tsunami events during historical and pre-historical times (e.g. Kelletat 1991, Pirazzoli et al. 1992, Stiros 2001, Shaw et al. 2008, Bruins et al. 2008). Crete is exposed to the Hellenic subduction zone in the south (Libyan Sea) and in the west (Ionian Sea) as well as to the Aegean volcanic arc and the Cretan Sea in the north. The Hellenic subduction zone has generated strong earthquakes, for example in AD 365 and AD 1303. Both earthquakes generated catastrophic supra-regional tsunamis that hit Crete's coasts as documented by geological evidence (Pirazzoli et al. 1992, Papadopoulos et al. 2007, Scheffers & Scheffers 2007, Bruins et al. 2008, Boulton & Whitworth 2017, Werner et al. 2018a, 2018b). Also during the Late Bronze Age (LBA), one of the largest volcanic eruptions in the Mediterranean took place on the Santorini (Thera) volcano. The eruption generated a tsunami that impacted the northern coast of Crete (Bruins et al. 2008, Werner et al. 2018b). These examples underline the high tsunami risk for the island. Tsunami events similar to the AD 365-type magnitude along the entire Hellenic subduction zone are supposed to reach a recurrence interval of 800 years (Shaw et al. 2008). Today, coastal areas of the Mediterranean are densely populated. Therefore, studying traces of palaeotsunami events is important to understand their impact on the Holocene coastal evolution and helps to assess the impact of possible future tsunami events.

Palaeotsunami traces in the Mediterranean have been identified as high-energy signatures in various types of sedimentary archives. First, sheets of translocated marine sands were found in near-coast silt-dominated lagoons or freshwater lakes (e.g., Aliki Lagoon, Greece: Kontopoulos & Avramidis et al. 2003, Voulkaria Lake, Greece: Vött et al. 2009, Thermaikos Gulf, Greece: Reicherter et al. 2010), locally associated with geomorphological forms of washover fans (Gargano coast, Italy: Gianfreda et al. 2001), or chevrons in case of high flow velocities and negligible influence of backflow erosion (e.g., Lefkada Lagoon, Greece: May et al. 2012, Gialova Lagoon, Greece: Willershäuser et al. 2015). Second, sheets of translocated marine sands are embedded in peat units deposited in paralic swamps (e.g., Cefalonia Island, Greece: Willershäuser et al. 2013, Evrotas River delta, Greece: Ntageretzis et al. 2015a). Third, mixed sedimentary units out of allochthonous and autochthonous material were identified in ancient harbour areas and corresponding deposits (e.g., Byzantine harbour of Yenikapı, Turkey: Bony et al. 2012, ancient harbour of Corinth, Greece: Hadler et al. 2013, Vött et al. 2018a, ancient harbour of Phalasarna, Greece: Pirazzoli et al. 1992, ancient harbour of Corfu, Greece: Finkler et al. 2018a, 2018b). Fourth, mixed, poorly sorted geoarchaeological units were identified as tsunami-related sediments deposited in archaeological contexts on land (e.g., Palaikastro, Greece: Bruins et al. 2008, Palairos/Pogonia, Greece: Vött et al. 2011a). Fifth, beachrock-type calcarenite in coast or near-coast positions turned out to have been deposited within the course of tsunami landfall and the sediments have been subject to post-depositional cementation (e.g., ancient harbour of Olympia at Pheia, Greece: Vött et al. 2011b, ancient harbour of Kyllini, Greece: Hadler et al. 2015, ancient harbour of Corinth and in the Diolkos area, Greece: Hadler et al. 2013). Finally, high-energy coarse-grained tsunami layers out of allochthonous material were also encountered in offshore sub-littoral and marine environments where they were entrained by local backwash currents (e.g., Caesarea, Israel:

Goodman-Tchernov et al. 2009, Tyuleneva et al. 2018, Augusta Bay, Italy: De Martini et al. 2010, Smedile et al. 2011, Mediterranean megaturbidite: Polonia et al. 2013).

However, despite this large variety of different tsunami traces, only few studies have been conducted so far in narrow, deeply incised valley systems, as for example at the Boca do Rio estuary, Portugal (e.g., Hindson et al. 1996 and Font et al. 2010 and references therein), although these valley systems are known to represent priority regions with regard to the maximum landward intrusion of tsunami waves. The latter was painfully experienced during the Indian Ocean 2004 and the Japan 2011 tsunami events (Adityawan et al. 2012, Tanaka et al. 2012, 2014, Tolkova & Tanaka 2016). In the Mediterranean, Ntageretzis et al. (2015b) detected palaeotsunami evidence in a valley to the northwest of Neapoli Vion, Vatika Bay (Greece), incised into older lithified Pleistocene fans and marine terraces. The inundation line was found to reach at least 400 m inland and Ntageretzis et al. (2015b) assumed funnelling and acceleration effects of the intruding tsunami waters. More recent observations from the Tōhoku-oki tsunami in 2011 documented that tsunamis following rivers and channels caused massive damage deep inland and are an important tsunami risk evaluation factor (Tanaka et al. 2014).

Focusing on the northern coast of Crete, the narrow and deeply incised Geropotamos River valley – facing the open Cretan Sea – was selected as a promising natural setting to search for palaeotsunami signatures in fluvial sedimentary archives. The main objectives of our study were (i) to search for extreme wave event (EWE) traces in the Geropotamos River sedimentary archives, (ii) to analyse EWE candidate deposits by using a multi-proxy geomorphological and sedimentological approach, (iii) to reconstruct potential EWE impacts and their flow dynamics in interaction with the Geropotamos River valley, and finally (iv) to compare the Geropotamos EWE signatures with signatures known from other coastal sites in search of supra-regional impacts along the northern coasts of Crete.

2 *Geography and tectonic setting*

2.1 *Tectonic setting*

Crete is located in close proximity to the Hellenic subduction zone. Here, the African plate is being subducted with 35–40 mm/y on average (McClusky et al. 2000, Reilinger et al. 2006, Hollenstein et al. 2008) beneath the Aegean microplate. A compressive accretionary wedge, the Mediterranean Ridge, has been developed above the subduction interface (McKenzie 1972, Le Pichon & Angelier 1979, Doutsos & Kokkalas 2001, Shaw & Jackson 2010). After Shaw & Jackson (2010), splay faults located in the accretionary wedge control the growth of Crete's topography by uplifting the overriding Aegean microplate. Within the last 13 million years, subduction and associated coseismic processes caused a cumulative uplift of Crete of approximately 2–3 km (McKenzie 1978, Meulenkamp et al. 1994, Jolivet et al. 1996). The central Iraklion ridge emerged first some 4 million years ago and the outer island parts followed ca. 1 million years later (Shaw & Jackson 2010). Studies by Tiberti et al. (2014) showed that in western Crete this net uplift includes periods of both uplift and subsidence.

Induced by the rollback effect of the subduction zone and its movement towards the south, a back-arc basin with an average water depth of 1000 m has been formed to the north of Crete (Angelier et al. 1982, McKenzie 1972, Doutsos & Kokkalas 2001, Reilinger et al. 2006,

Fig. 1. Overview of the lower course of the Geropotamos River and the river mouth area into the Cretan Sea (A). Detail maps of the Geropotamos River mouth area (B) and the inactive external bank further inland (C) show locations of vibracoring sites and ERT transects. Isolines in inset map of Crete depict amount of coseismic uplift associated with AD 365 earthquake in meters (after Kelletat 1991, Shaw et al. 2008). Maps based on Google Earth 2017.

Seidel et al. 2007, Royden & Papanikolaou 2011). The Hellenic subduction interface dips northwards at 10° to 15° whereas the subducted slab reaches depths of 35 to 45 km beneath Crete and several hundreds of kilometres beneath the central Aegean (e.g., Bohnhoff et al. 2001, van Hinsbergen et al. 2005, Hollenstein et al. 2008). A well-defined Benioff seismic zone reaches a maximum depth of 200 km and ends underneath the volcanic back-arc of the Cyclades including the still active Colombo-complex near Santorini and Milos (Le Pichon & Angelier 1979, Hollenstein et al. 2008). During Miocene, crustal extension of the overriding Aegean

microplate started and lead to a fragmentation of Crete into fault-bounded blocks creating a horst-and-graben structure (Angelier et al. 1982, Peterek & Schwarze 2004, Seidel et al. 2007, Caputo et al. 2010, Mason et al. 2016). The extensional faulting along the Hellenic Trench is accompanied by frequent shallow earthquakes whereas deeper earthquakes are triggered by the descent of the underlying plate subject to subduction (Taymaz et al. 1990, Papazachos et al. 1997).

During history, Crete was hit by several catastrophic seismic events such as the prominent tsunamigenic earthquake that occurred on 21 July AD 365. This earthquake was triggered by a N–E dipping reverse fault located within the overriding plate in the south of Crete (Shaw et al. 2008, Lorito et al. 2008, Flouri et al. 2013) and reached an estimated magnitude of $M_w = 8.3$ (Stiros 2001, Shaw et al. 2008, Shaw & Jackson 2010). During this earthquake, the western and southwestern parts of Crete experienced coseismic crust uplift of up to 9 m (Fig. 1). Today, the pre-AD 365 sea level stand is still visible as well preserved bio-erosive markers and algal rims along the coasts of western Crete (e.g., Spratt 1865, Pirazzoli et al. 1982, 1996, Shaw et al. 2008, Mouslopoulou et al. 2015). Another strong earthquake (ca. Mw = 8.0) took place on 8 August AD 1303 and ruptured the eastern part of the Hellenic Arc between Crete and Rhodes (Papadopoulos et al. 2007). Based on several historical documents, an associated tsunami reached Crete's northeastern coast and struck the capital city of Heraklion (Papadopoulos et al. 2007, 2014). During the last century, the strongest tsunamigenic earthquake was generated at a 40 km-long active fault in 1956 offshore Armorgos Island and reached a magnitude of Mw = 7.5 (Nomikou et al. 2018). A detailed overview of all known historical and prehistorical tsunami records in the Mediterranean are listed in earthquake and tsunami catalogues (e.g., Galanopoulos 1960, Papadopoulos & Chalkis 1984, Tinti 1991, Guidoboni et al. 1994, Soloviev et al. 2000, Ambraseys 2009, Hadler et al. 2012, Papadopoulos et al. 2014).

2.2 *Geographical setting of the study area*

The study area is located at the north coast of Crete in the lower course of the Geropotamos River. The study area is between the cities of Rethymnon in the west and Heraklion in the east near the villages of Lavris and Panormos (Figs 1A–C and 2). This region was unaffected by the coseismic uplift of the AD 365 earthquake (Fig. 1A, Kelletat 1991). The Geropotamos River reaches a length of 47 km and its catchment area amounts to 40 km^2 (Sdao et al. 2012). In the lower course of the river (Fig. 2), the valley meanders are deeply incised into limestones and dolomites of the Tripolitza unit (Jurassic-Eocene limestones overlying the Tyros or Ravdoucha beds comprising Permo-Triassic shales, phyllites, and quartzites) as well as into overthrusted Phyllite-Quarzites including the Arna unit (IGMR 1977, Papanikolaou & Vassilakis 2010). Deeply incised river beds in general indicate increased fluvial erosional processes induced by uplifting land masses or low sea levels. The study area is further characterized by major NW–SE/NNW–SSE running faults (IGMR 1977) which seem to be responsible for the overall flow direction of the Geropotamos River. Another fault system trends towards SW–NE.

Studies in the Geropotamos River valley were conducted in two different areas. First, at the immediate river mouth on top of a pronounced beach ridge and associated washover fans, reaching up to 100 m inland. Second, in an area located ca. 1 km upstream in a former exter-

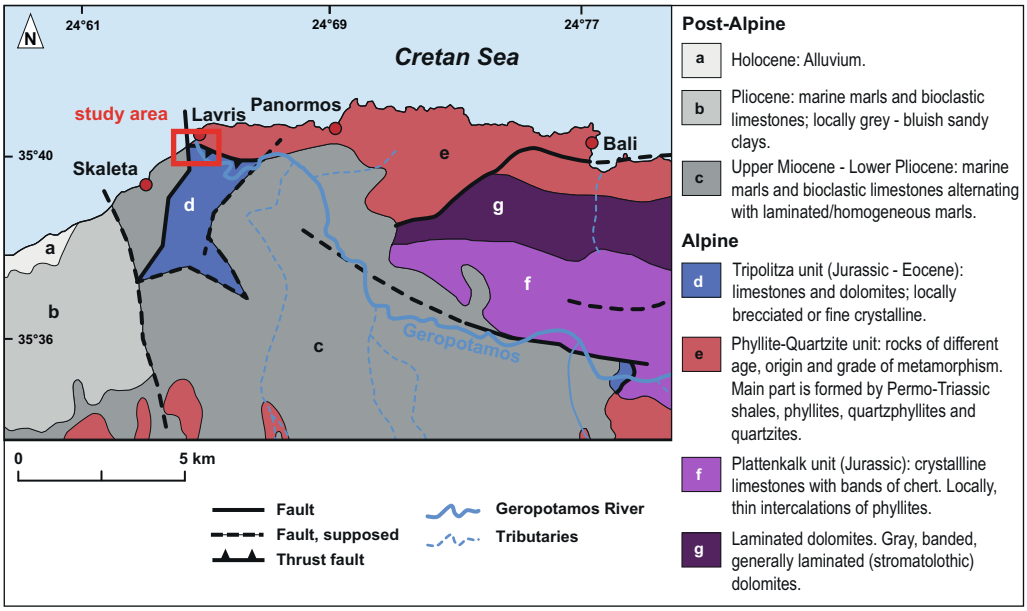

Fig. 2. Geological map of the Geropotamos River study area, northern Crete, showing geotectonic units. Red box marks location of the study area. Map adapted from IGMR (1977), Papanikolaou and Vassilakis (2010).

nal bank position of the Geropotamos River. This undercut slope is presently inactive and lies today at an elevation of ca. 6 m above sea level (m a.s.l.) and approximately 110 m distant from the present river course. The latter runs at an elevation of ca. 3 m a.s.l. Geomorphological and geophysical investigations were carried out at the slope of the southern valley flank, exposed to the northwest and out of reach of present fluvial processes. Between the two study sites, the valley floor is only 100 m to 250 m wide.

3 *Material and methods*

3.1 *Field work*

Geophysical prospection was carried out using electrical resistivity tomography (ERT) in order to pre-examine the bedrock topography and main stratigraphic structures of the near-surface underground. We used a multi-electrode Syscal R1 + Switch 48 device (type Iris Instruments) with a Wenner-Schlumberger electrode array. Measured data were inverted into depth sections using the RES2DINV software (Geotomo Software). Local stratigraphic data were obtained based on vibracores that were also used to calibrate the results of the ERT measurements. Vibracores were drilled with a closed auger system using a Cobra Pro handheld coring device (type Atlas Copco) and plastic inliners (50 mm in diameter). Vibracore GER 3A was also drilled with an open auger system and was used for microfossil sampling (GER 3). Position and elevation

data of ERT electrodes and vibracoring sites were measured with a differential GPS (Topcon Hiper Pro FC-250), reaching a minimum horizontal and vertical precision of 2 cm.

3.2 *Laboratory analyses*

Sediment-filled plastic inliners were cut into halves in the geolaboratory of the Johannes Gutenberg-Universität Mainz, Germany. The core halves were cleaned, photographically documented, and analysed. Selected sediment samples (GER 3A: 37 samples, GER 4A: 71 samples) were retrieved from representative stratigraphic units for further sedimentological analyses. Samples for micropalaeontological studies were retrieved from vibracore GER 3, the open drilled version of vibracore GER 3A.

Grain size analyses of sediment samples were conducted using the sieve and pipette method after Köhn (Köhn 1929, DIN/EN ISO 11277 2002). Standard pre-treatment included dry-sieving in order to determine the amount of coarse particles with diameter > 2 mm, followed by 12 hour-peptisation of the fraction < 2 mm in sodium pyrophosphate. Percentages of eight grain size classes (clay: < 2 µm, fine silt: 2–6.3 µm, medium silt: 6.3–20 µm, coarse silt: 20–63 µm, finest fine sand: 63–125 µm, fine sand: 125–200 µm, medium sand: 200–630 µm, coarse sand: 630–2000 µm) were determined. Based on a 99-step cosine interpolation function over the grain size classes, (mean) relative frequency distribution curves as well as cumulative frequency curves were calculated for each sample.

The geochemical element composition of sediments (in total 32 elements) was analysed using a portable Niton XL3t 900 S GOLDD XRF handheld analyser (calibration mode SOIL) in vertical steps of 2 cm along the entire cores. The results of the portable XRF (PXRF) technique are semi-quantitative and commonly used to identify trends and changes in geochemical composition between different sediment units (Chaguć-Goff et al. 2010, 2017, Vött et al. 2011a, Finkler et al. 2018b, Judd et al. 2017). We used the calcium (Ca)/iron (Fe) ratio in order to differentiate between marine and terrestrial depositional conditions and abrupt environmental changes. Increased iron contents are often associated with terrestrial weathering processes; on the contrary, increased calcium contents are associated with marine input in terms of biogenic marine carbonate, such as marine micro- and macrofauna shells (Vött et al. 2011a, 2015, Chaguć-Goff et al. 2014, 2017). However, it is necessary to consider the influence of carbonate bedrock material and anthropogenic effects that may influence these signals (Vött et al. 2015).

A spectrophotometer (Konica Minolta CM-600 d) was used to quantify sediment colour based on the chromaticity values a* and b* of the CIELAB colour space (L*a*b*) with measurements every 2 cm. The variables a* and b* specify the portion of red (+a*) and green (-a*) and yellow (+b*) and blue (-b*) of the overall sediment colour. The sediment colour can be used as an additional tool to discriminate between sedimentary facies, for example to differentiate between sediments accumulated under oxic or anoxic conditions or to highlight differences in the organic content. The magnetic susceptibility of sediments, the content of diamagnetic and magnetic materials of the sediment, was measured in 1 cm steps using a Bartington MS2K surface sensor.

The microfossil content of selected sediment samples (GER 3/3A: 21 samples, GER 4A: 57 samples) was analysed using a semi-quantitative approach in order to reconstruct

palaeoenvironmental changes and to differentiate between autochthonous and allochthonous deposits. As preparation for the microfossil analyses, 15 ml of each sample were first sieved in different fractions (> 400 µm, 400–200 µm, 200–125 µm, and < 125 µm) and then analysed with the help of a stereomicroscope (Nikon SMZ 745T). Genera and, if possible, species of foraminifera tests were determined after Cimerman & Langer (1991), Murray (2006) and Rönnfeld (2008). In some cases, foraminifera tests were strongly calcified and worn and the species was not determinable. Z-series photos of foraminifera specimens were taken with a light-polarizing microscope (Nikon Eclipse 50i POL with Digital Sight DS-FI2 digital camera).

Six samples underwent ^{14}C AMS radiocarbon analysis for geochronological information. We only used plant remains for dating and refrained from choosing marine fossils because of the marine reservoir effects, whose species-specific influence in space and time is still unknown (for further details see discussion Vött et al. 2018a, 2018b). Conventional radiocarbon ages were calibrated using the calibration software Calib Rev 7.10 and the Marine13 and IntCal13 datasets (Reimer et al. 2013).

4 *Results*

4.1 *Geropotamos River mouth area*

4.1.1 *Pre-coring ERT survey*

We carried out three ERT transects in the river mouth area (Fig. 3) for a pre-coring exploration of the near-surface underground. The location and the course of the ERT transects is shown in Fig. 1B. All ERT depth sections were converted to the same scale comprising electrical resistivity values from 1 (dark blue) to > 220 Ωm (purple). Additionally, the ERT depth sections include the position of vibracoring site GER 4A and the related stratigraphy. In general, high resistivity values reflect coarse-grained sand and gravel, partly (very) dry above groundwater level, or bedrock. Low resistivity values indicate fine-grained material, mostly silt and clay, and/or water saturated sediments.

ERT transect GER ERT 3 starts at the present shore and runs in a NW-SE direction across the beach ridge to the distal end of a recent washover fan. ERT transects GER ERT 4 and 5 run perpendicular to the flow direction of the Geropotamos River, namely where the beach reaches its highest elevations and in a distal position of the washover fan, respectively. Depth sections GER ERT 3 and 4 show a two-part horizontal composition with (very) low resistivity values (mostly < 5 Ωm) in the lower part reaching up to ca. 0 m a.s.l., and higher resistivity values at the top (> 42 Ωm). The depth section GER ERT 5 shows a similar composition as transects GER ERT 3 and 4, but with higher electrical resistivity values in the western end of the transect. Furthermore, the depth section of GER ERT 5 shows high to very high values (42 to > 220 Ωm) in the top zone, which appears somewhat incised into the underlying part with lower resistivity values.

4.1.2 *Multi-proxy analysis of vibracore GER 4A*

Vibracore GER 4A was drilled ca. 80 m inland at an elevation of 1.60 m a.s.l. behind the present beach ridge and on top of a washover fan (Figs 1B and 3). The vibracoring site is situated 43 m

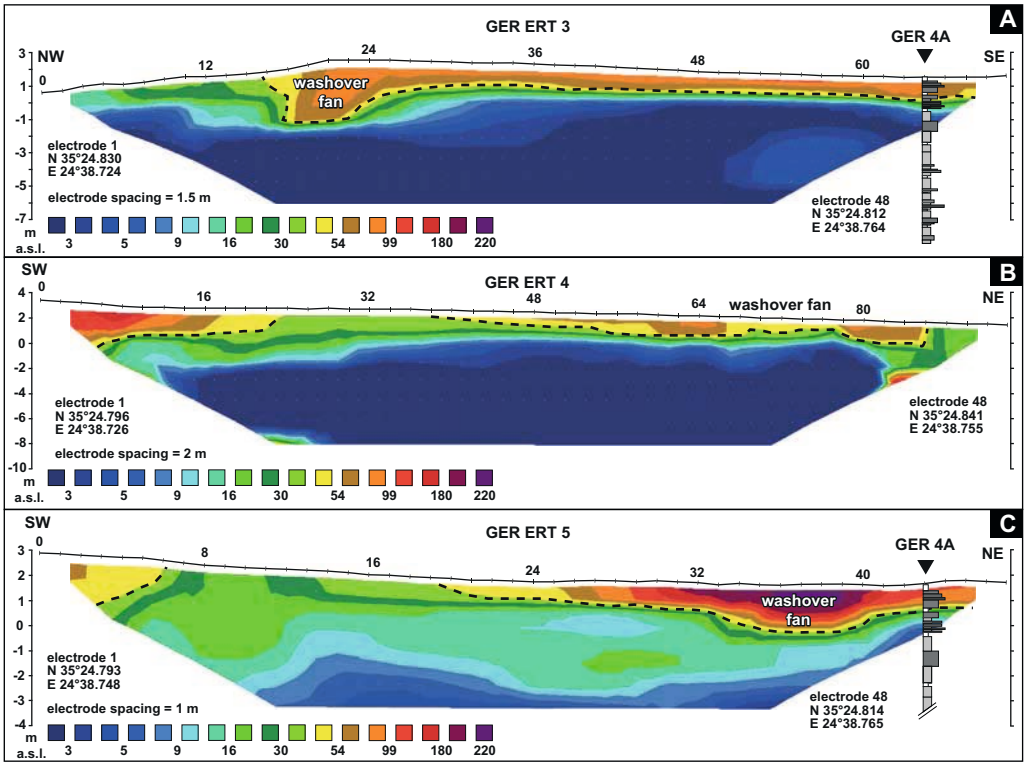

Fig. 3. ERT depth sections realized within the frame of geophysical prospection in the Geropotamos River mouth area. See text and Fig. 1 for further explanation.

from the beginning of transect GER ERT 5 and is situated quite in the middle of the entrance of the deeply incised Geropotamos River valley in the east. To the north of the coring site GER 4A, the Geropotamos River discharges into the Cretan Sea. We used a closed auger drill system and reached a maximum coring depth of 10 m below surface (m b.s.). To classify the stratigraphic record of GER 4A, we differentiate between five stratigraphic units inferred from sedimentological criteria namely grain size, sediment colour and macrofossil content (Table 1).

The stratigraphic record of vibracore GER 4A (Fig. 4 and Table 1) from 10.00 to 2.10 m b.s. (-8.4 m b.s.l. to 0.50 m a.s.l., b.s.l. = below sea level) is dominated by clay and silt, greyish and brownish in colour (units I and IV), that partly contain a higher sand content. These fine-grained deposits are intersected by six distinct layers, namely from 9.78 to 9.52 m b.s. (-8.18 to -7.92 m b.s.l.), 8.80 to 8.46 m b.s. (-7.20 to -6.86 m b.s.l.), 7.54 to 7.36 m b.s. (-5.94 to -5.76 m b.s.l.), 6.81 to 6.73 m b.s. (-5.21 to -5.13 m b.s.l.), 5.66 to 5.52 m b.s. (-4.06 to -3.92 m b.s.l.), and 5.34 to 5.25 m b.s. (-3.74 to -3.65 m b.s.l.) by predominantly greyish to light-greyish fine and medium sand (unit II). Each intersecting layer shows a sharp erosional contact to the underlying deposits and visible marine shell fragments. Two layers of greyish-beige coarse sand and (fine) gravel (unit III) intersect the dominant clay and silt sequence from 7.82 to 7.66 m b.s. (-6.22 to -6.06 m b.s.l.) and from 6.71 to 6.66 m b.s. (-5.11 to -5.06 m b.s.l.). At 3.26 to 2.65 m b.s. (-1.66 to -1.05 m

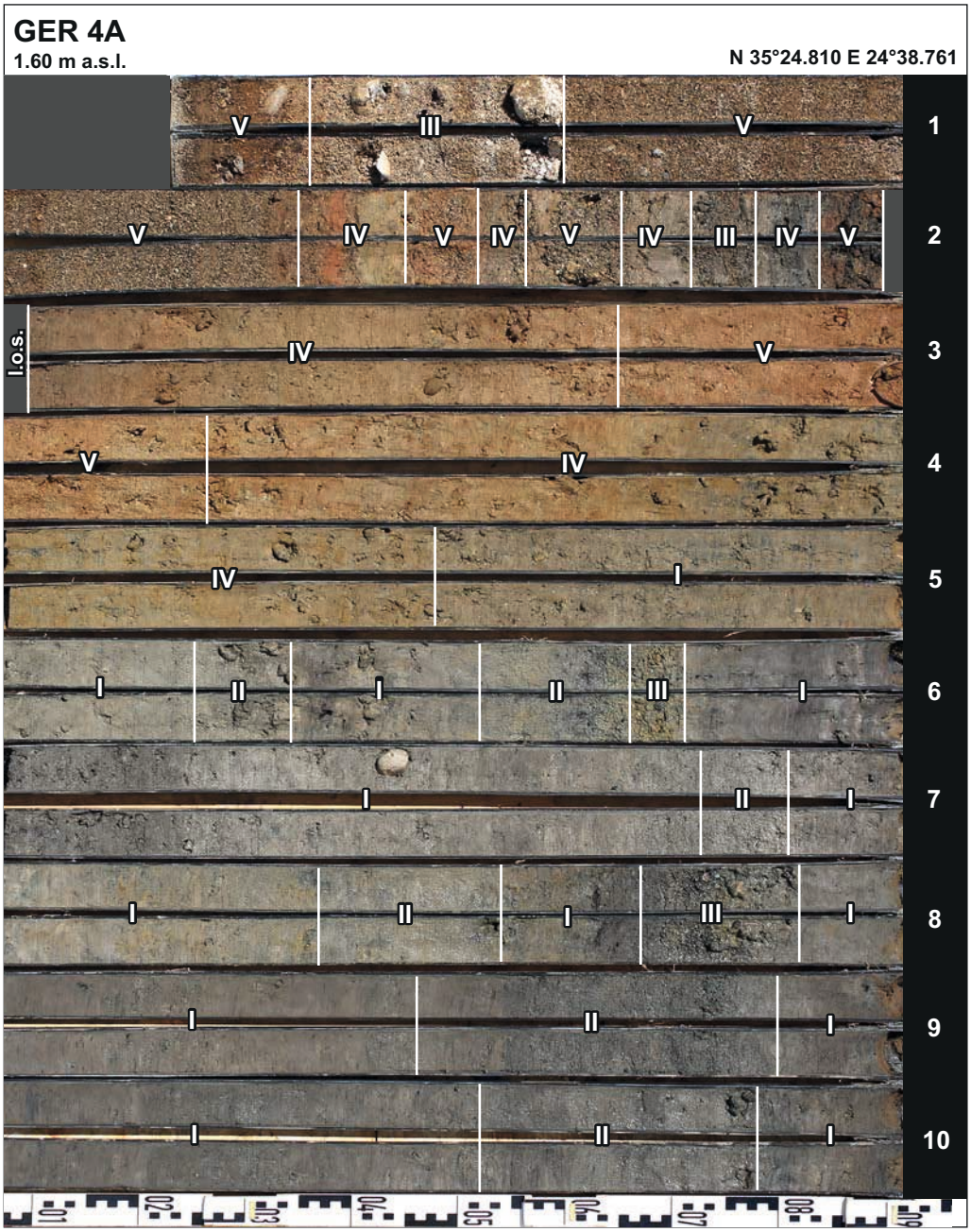

Fig. 4. Photo of sediment core GER 4A drilled in the Geropotamos River mouth area, ca. 80 m distant from the present-day shoreline. Sedimentary units I to V are based on grain size, colour, and macrofossil content. See text and Table 1 for explanation.

Table 1. Stratigraphic units found for vibracores GER 4A and GER 3A based on grain size data, sediment colour, and macrofossil content.

Unit	Sediment character		
	Grain size	**Colour**	**Macrofossil content**
I	clay and silt, partly with higher sand content	dark grey to light grey	
II	fine and medium sand	grey to light grey-beige (GER 4A), red-brown (GER 3A)	marine shell fragments
III	coarse sand to (fine) gravel	grey to beige (GER 4A), red-brown to multicoloured (GER 3A)	marine shell fragments
IV	clay and silt	reddish-beige and gray parts	
V	medium and coarse sand	reddish-beige to reddish-dark grey	marine shell fragments
VI	silt and fine sand, partly higher sand content	greyish-brown	
VII	clay and silt, slate and glimmer fragments	brownish-red	
VIII	clay and silt, roots	dark brown	

b.s.l.) reddish-beige coloured medium and coarse sand with marine shell fragments disrupt the clay and silt sequence in the upper part of the vibracore (unit V). Following a loss of sediment, we found an alternating layering of deposits of units III, IV, and V from 1.90 to 1.35 m b.s. (-0.30 bsl to 0.25 m a.s.l.). This section is covered by a massive layer out of well-sorted reddish-brown medium and coarse sand (unit V) that reaches up to the present-day's surface. Between 0.60 m b.s. and 0.36 m b.s. (1.00 to 1.24 m a.s.l.), it is intersected by coarse-grained sand and gravel deposits of unit III.

The stratigraphic record of vibracore GER 4A is shown in Fig. 5 together with selected sedimentary and geochemical parameters. The Ca/Fe log shows maximum values for coarse-grained units (III, IV, and V), indicating an increased input of Ca in the upper section of the vibracore. On the contrary, coarse-grained units found in the lower core section show positive as well as negative peaks and a general trend is not discernible. Maximum magnetic susceptibility values and some secondary peaks are associated with coarse-grained layers (units II and III) in the lower core section, but do not show a general trend. With beginning of unit IV up to present-day's surface, the magnetic susceptibility increases and shows higher values on average than in the rest of the core. The a*/b* CIELAB colour ratio traces the transition from greyish to reddish-brown deposits at ca. 3.7 m b.s. (-2.1 m b.s.l.). Three peaks indicate the increase of reddish-brown colours in the upper core section. The results of the grain size analyses neatly reflect the stratigraphic structure of the core. Each coarse-grained unit (II, III, and V) shows an increasing percentage of sand (subdivided in coarse sand, medium sand, and fine sand). Coarse components with diameters > 2 mm were found for units II and III of the lower core, from ca. 1.90 m b.s.(-0.3 m b.s.l.) upwards, the percentage of coarse-grained deposits, especially the percentage of coarse and medium sand, and components with diameters > 2 mm strongly increases.

The mean relative frequency distribution and the mean cumulative frequency of sample-specific grain sizes for each sedimentological unit are depicted in Fig. 6. Units I and IV are

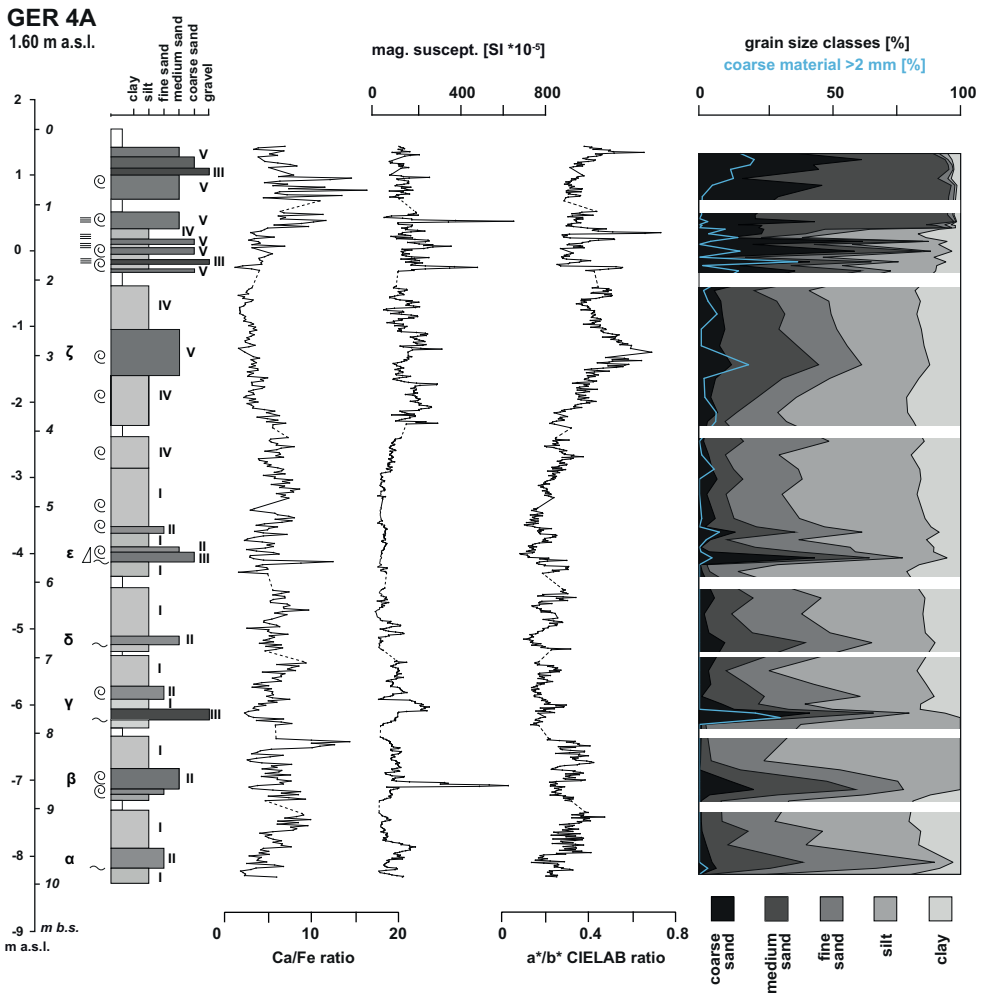

Fig. 5. Stratigraphic log of vibracore GER 4A compared with selected palaeoenvironmental proxies. Cumulative grain size data refer to fine sediment < 2 mm (sum = 100 %) and coarse sediment > 2 mm (blue line, percentage referred to total mass of sample).

dominated by coarse silt and clay. In some samples of unit I and most samples of unit IV there is also a maximum for medium sand, resulting in an overall moderate grade of sorting. In contrast, samples from units II, III, and V show a clear maximum in the sand fraction and are predominantly characterised by medium sand (units II and V) and medium to coarse sand (unit III). However, the mean relative frequency distribution of units II, III, and V shows several secondary maxima, indicating a poor sorting of the deposits.

The semi-quantitative evaluation of the microfossil content is depicted in Fig. 7. Studied samples (black and white triangles to the right of the vibracore log) are consecutively numbered from top to base. A selection of foraminifera species and other microfossils found

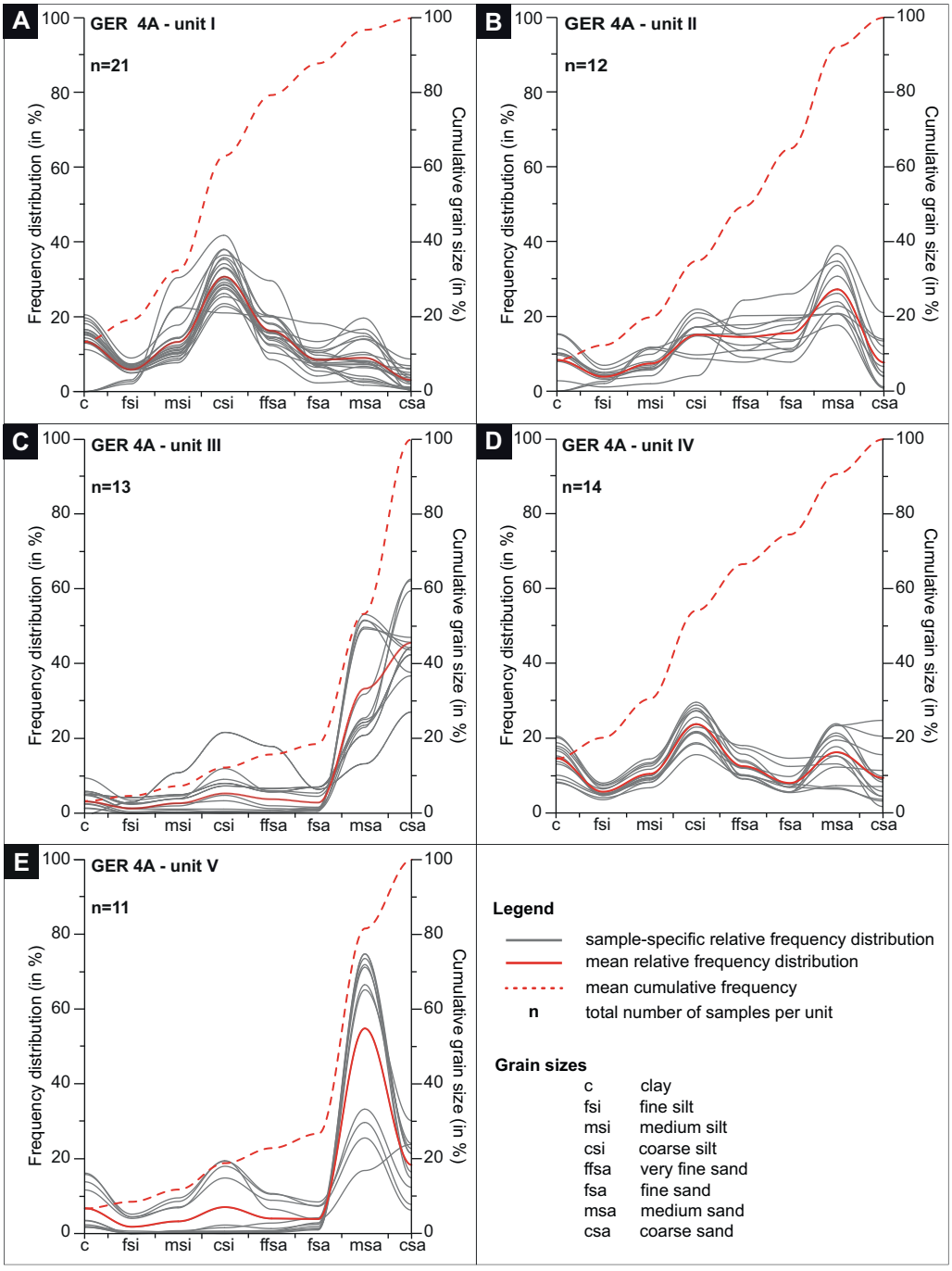

Fig. 6. Relative frequency distribution curves of grain size data obtained for sediment samples from vibracore GER 4A classified by stratigraphic units I to V. See Table 1 and text for further explanation.

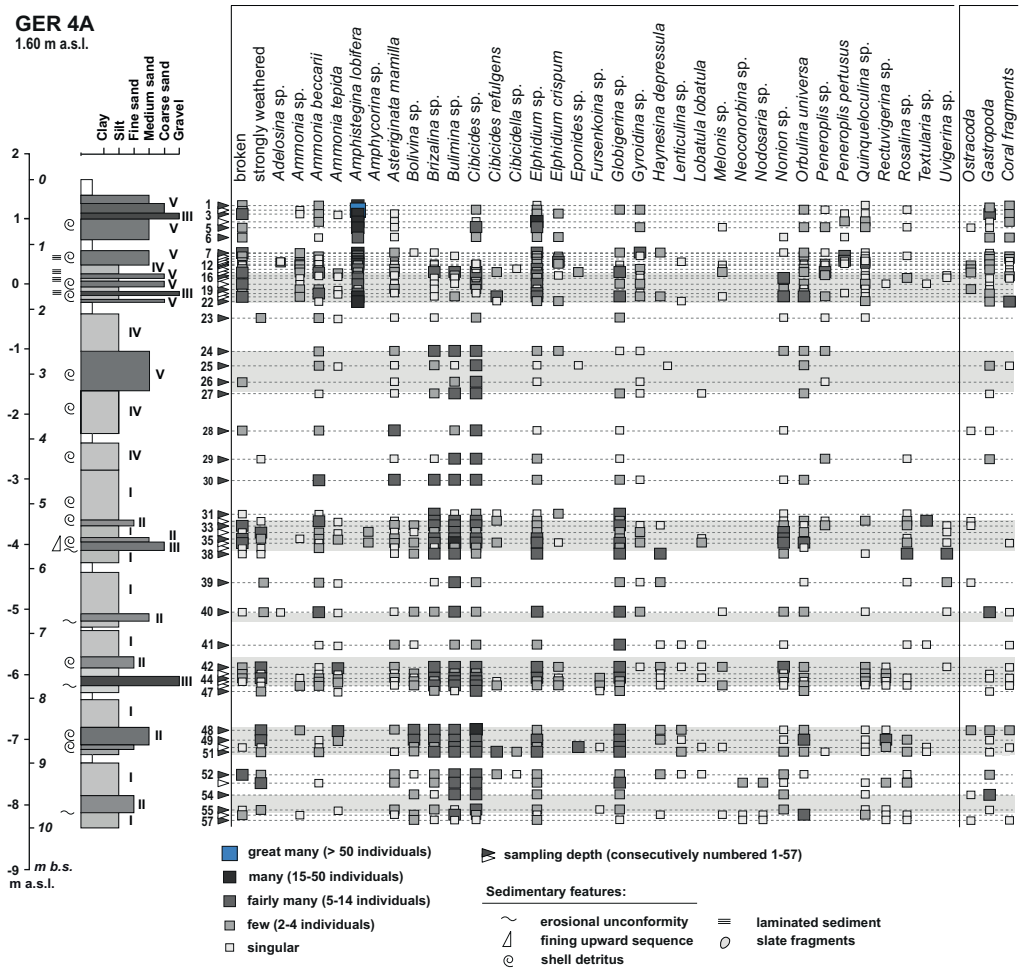

Fig. 7. Semi–quantitative results of microfossil analysis of sediment samples from vibracore GER 4A. Triangles near scale bar indicate sampling depth of individual samples. Triangles are numbered consecutively from top to base (1 to 57). I to V indicate stratigraphic units. See text, Fig. 6 and Table 1 for further explanation.

typical of vibracore GER 4A is shown in Fig. 8. Concerning the abundance and the diversity of foraminifera species, the vibracore shows a three-part division. The lower part of the core generally shows a high abundance and high diversity of found foraminifera species. In the middle part, approximately starting with the appearance of unit IV, abundance and diversity are relatively lowest but increase again towards the top. Maximum abundance and maximum diversity of foraminifera genera is rather associated with coarse-grained sedimentary units (units II, III, and V) than with fine-grained deposits (units I and IV). The foraminiferal assemblage of unit I includes species, such as *Ammonia beccarii*, *Ammonia tepida*, *Haynesina depressula*, and several ostracods that are associated with brackish habitats, as for example

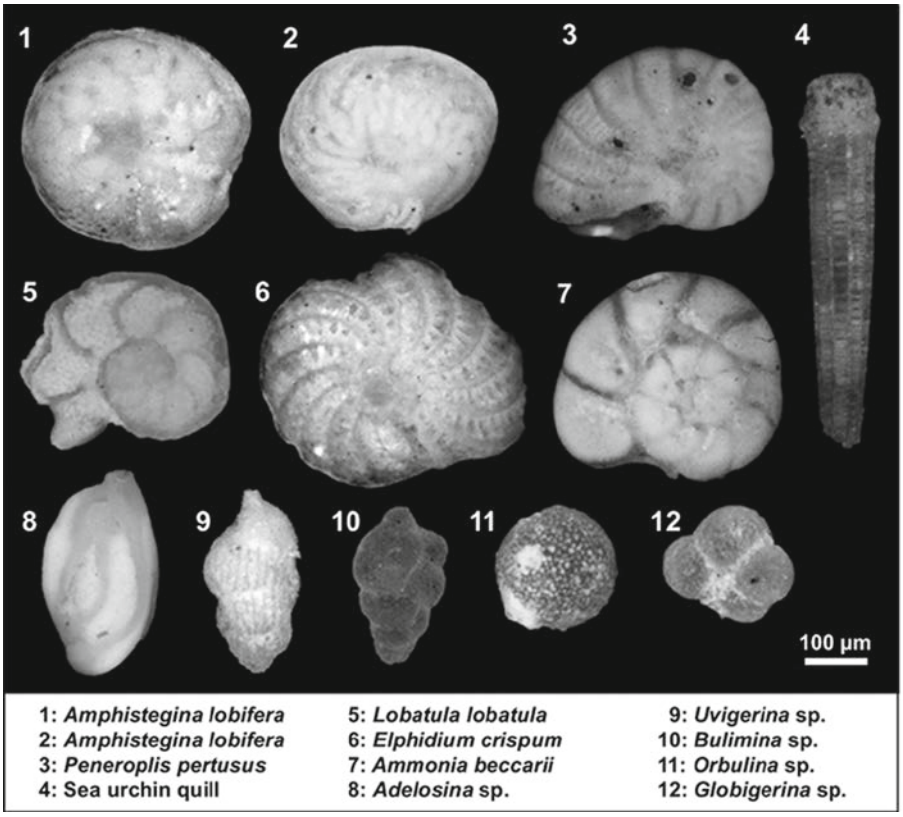

Fig. 8. Scanning electron microscope photos of selected foraminifera specimens and other microfossils found in samples from vibracore GER 4A.

those of lagoons. The existence of foraminifera that prefer shallow marine habitats, for example *Asteriginata mamilla*, *Nonion* sp., and *Rosalina* sp., indicate constant influence of saltwater. Several shallow marine to fully marine (cold marine) species almost exclusively occur in units II, III, and V, namely *Cibicides refulgens*, *Cibicidella* sp., *Elphidium crispum*, *Fursenkonia* sp., *Lobatula lobatula*, *Quinqueloculina* sp., and *Uvigerina* sp. Additionally, coral fragments can be predominantly found in these units. Other foraminifera species such as *Bulimina* sp., *Cibicides* sp., *and Globigerina* sp. occur as a kind of background noise, showing no specific change in abundance. Specimens of *Amphistegina lobifera* were only found in top-core position. They occur for the first time in sample 22 at 1.20 m b.s. (0.40 m a.s.l.).

4.2 *Geropotamos River valley area further inland*

4.2.1 *Pre-coring ERT survey*

The depth sections GER ERT 1 and GER ERT 2 of the geophysical exploration realized ca. 1 km further inland from the river mouth are depicted in Fig. 9. ERT depth sections were converted

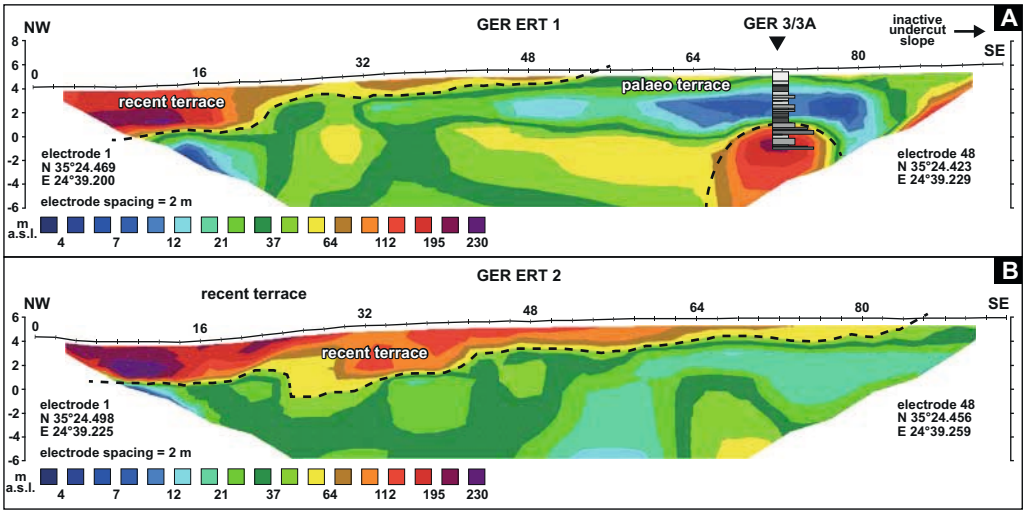

Fig. 9. ERT depth sections realized within the frame of geophysical prospection in the environs of an inactive external bank of the Geropotamos River further inland. See text and Fig. 1 for further explanations.

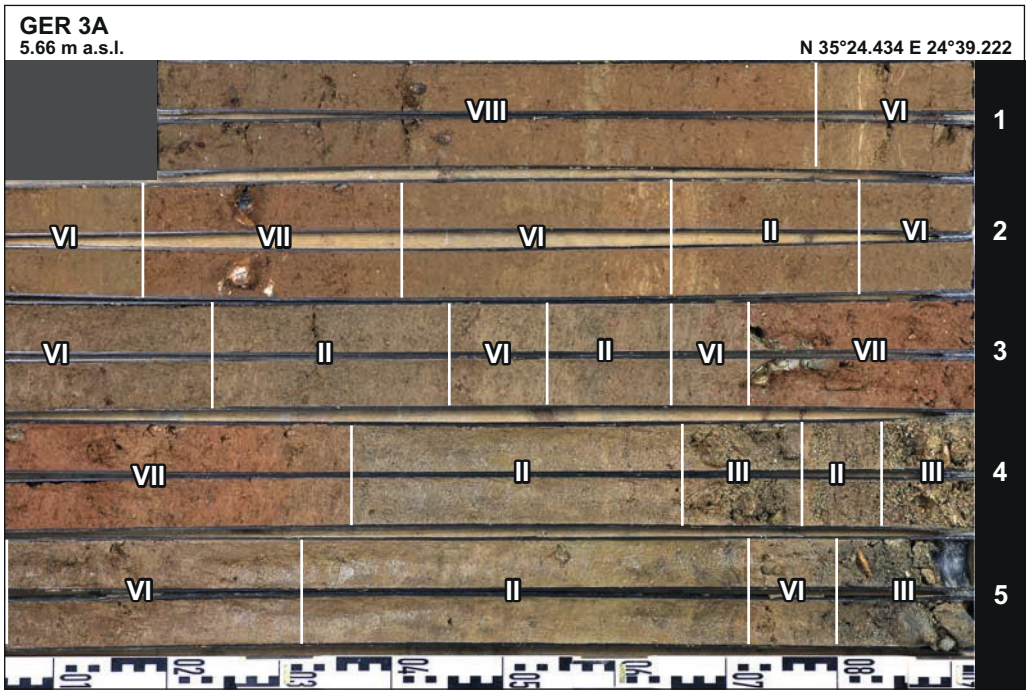

Fig. 10. Photo of sediment core GER 3A drilled on an inactive external bank of the Geropotamos River valley area ca. 1 km inland. Sedimentary units I to VIII are based on grain size, colour, and macrofossil content. See text and Table 1 for explanation.

to the same scale comprising electrical resistivity values from 1 Ωm (dark blue) to > 230 Ωm (purple). Both transects start near the present river bed and run in a NW-SE direction across the inactive undercut slope of the Geropotamos River (see Fig. 1C). They show a more or less two-part horizontal composition with little resistivity values in the lower part (1 to ca. 50 Ωm), speaking for moderate- to fine-grained deposits. In contrast, the upper part is characterised by maximum electrical resistivity values (> 50 Ωm) probably associated with coarse-grained deposits. Moreover, the southeastern part of depth section GER ERT 1 is characterised by another zone of higher resistivity values below the present sea level, most probably representing a distinct zone of coarse-grained sediments.

4.2.2 *Multi-proxy analyses of vibracore GER 3A*

Vibracoring site GER 3A is located ca. 1 km distant from the present-day shoreline, at 72 m of transect GER ERT 1 (Fig. 1). Vibracore GER 3A, drilled at 5.66 m a.s.l. on a former external bank of the Geropotamos River, reached a maximum drilling depth of 5 m b.s. (0.66 m a.s.l.). Its stratigraphic record can be divided into five stratigraphic units (Fig. 10, Table 1) inferred from grain size data, sediment colour, and visible macrofossil content. The core is predominantly characterised by alternating beige and grey sediment layers consisting of sand and gravel (units II and III) and of clay, silt and fine sand (units VI, VII and VIII). Between 3.36 and 2.72 m b.s. (2.30 to 2.94 m a.s.l.) and between 1.41 and 1.18 m b.s. (4.25 to 4.48 m a.s.l.), clayey and silty deposits include multiple slate and other crystalline bedrock fragments and show a reddish-brown colour (Fig. 11).

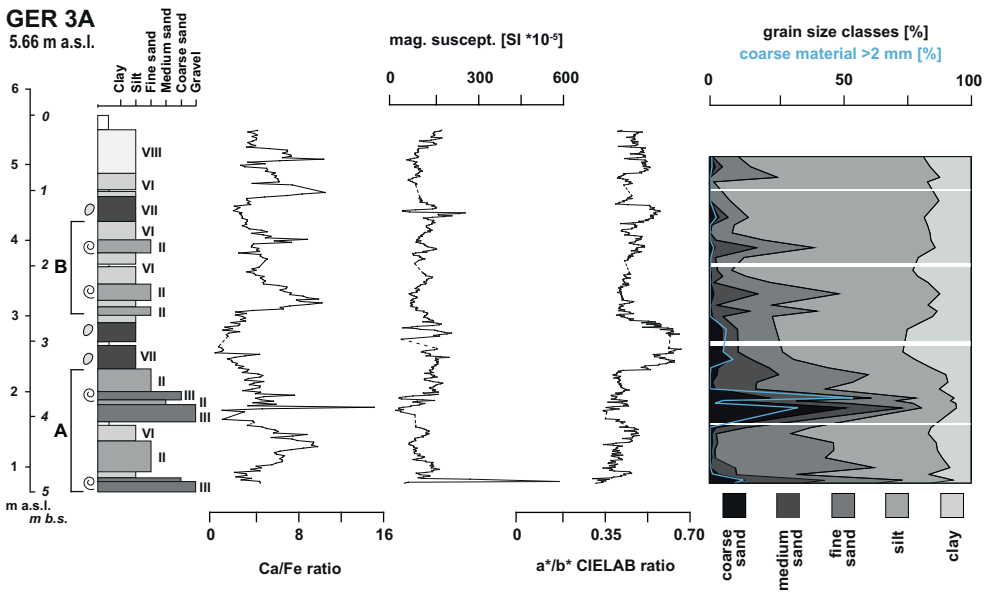

Fig. 11. Stratigraphic log of vibracore GER 3A compared with selected palaeoenvironmental proxies. Cumulative grain size data refer to fine sediment < 2 mm (sum = 100 %) and coarse sediment > 2 mm (blue line, percentage referred to total mass of sample).

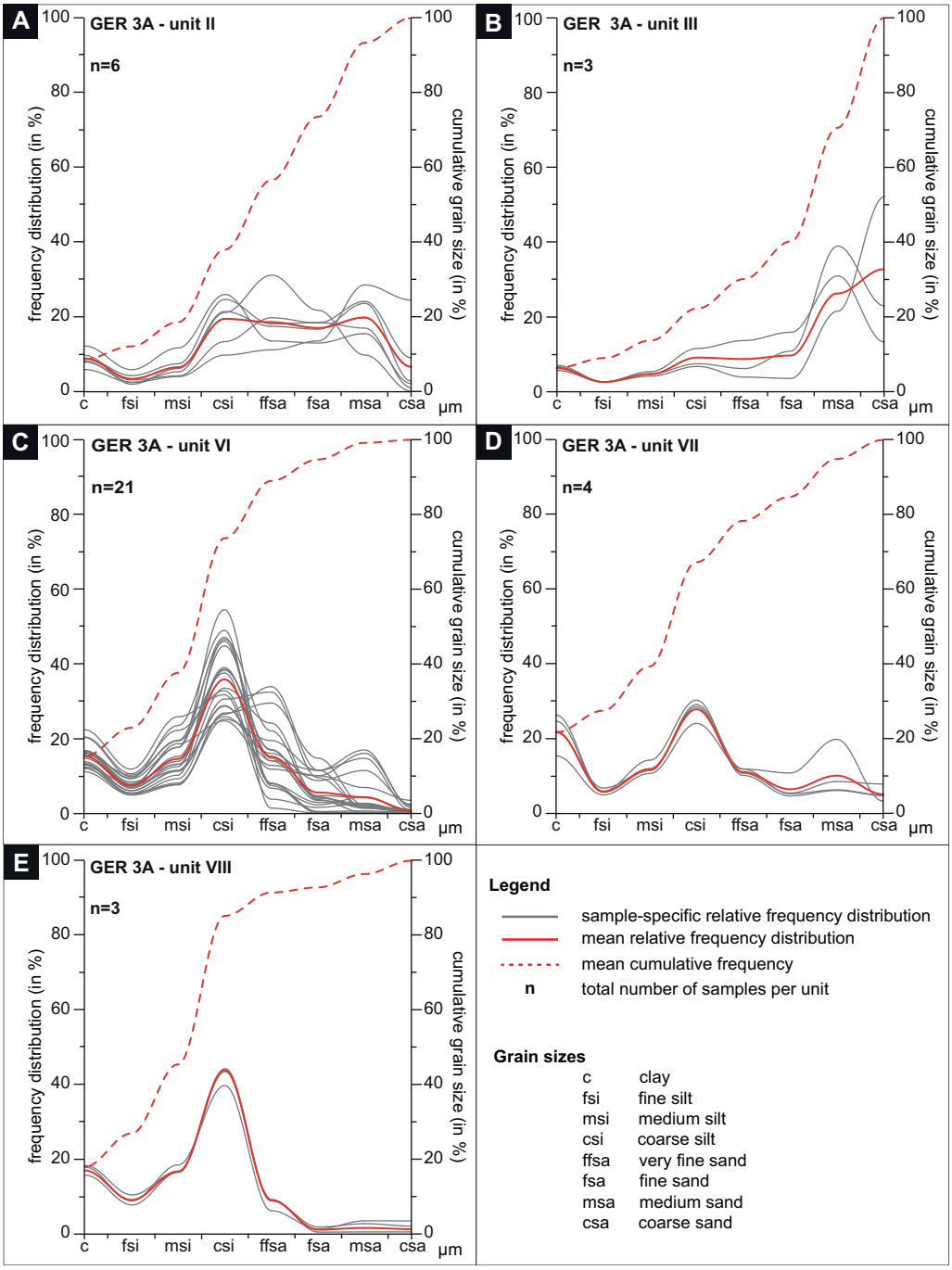

Fig. 12. Relative frequency distribution curves of grain size data obtained for sediment samples from vibracore GER 3A classified by stratigraphic units II to VIII. See Table 1 and text for further explanation.

Selected sedimentary and geochemical parameters are summarised in Fig. 11. The Ca/Fe ratio shows highest values predominantly associated with coarse-grained units II and III, except for top-core samples. On the contrary, the magnetic susceptibility values do not reveal a specific trend. Highest values are related to unit III deposits in the lowermost part of the core. Two secondary peaks are associated with unit VII deposits. The colour spectroscopic analysis of GER 3A highlights unit VII sediments with their reddish-brown sediment colour: Between 3.36 and 2.72 m b.s. (2.30 to 2.94 m a.s.l.) and between 1.41 and 1.18 m b.s. (4.25 to 4.48 m a.s.l.), the increasing a*/b* CIELAB ratio shows higher values indicating higher contents of reddish-brown material. Maximum sand amounts were found for units II and III , in particular coarse sand in units III, in the lower part of the sediment core. Maximum percentages of skeletal components are also associated with unit III deposit. In contrast, from 3.36 m b.s. (2.30 m a.s.l.) towards the present surface, silt and clay represent at least 50–75 % of all clasts. The Fig. 12 depicts mean relative frequency grain-size distribution curves for each unit. Sand-dominated unit II shows the poorest sorting of all units with an average of ca. 20 % for all grain sizes between coarse silt and medium sand. Unit III, only with a slightly better sorting, shows a maximum of coarse sand (30 %). Units VI and VIII contain up to 40 % coarse silt and show a secondary maximum for clay

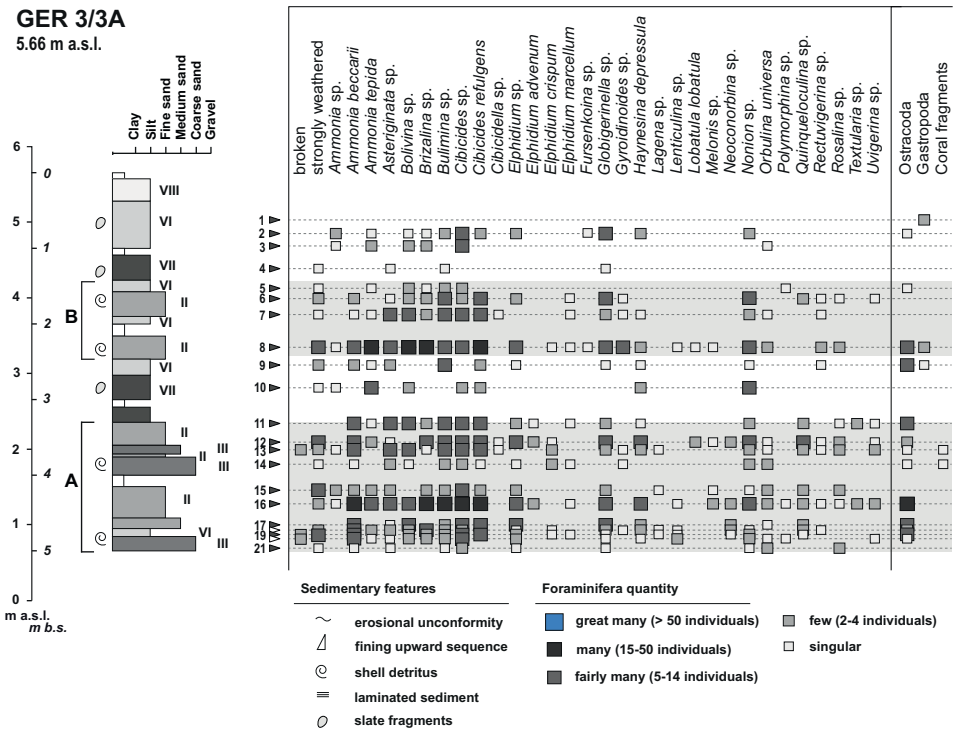

Fig. 13. Semi-quantitative results of microfossil analysis of sediment samples from vibracore GER 3A. Triangles near scale bar indicate sampling depth of individual samples. Triangles are numbered consecutively from top to base (1 to 21). II to VIII indicate stratigraphic units. See text, Fig. 6 and Table 1 for further explanation.

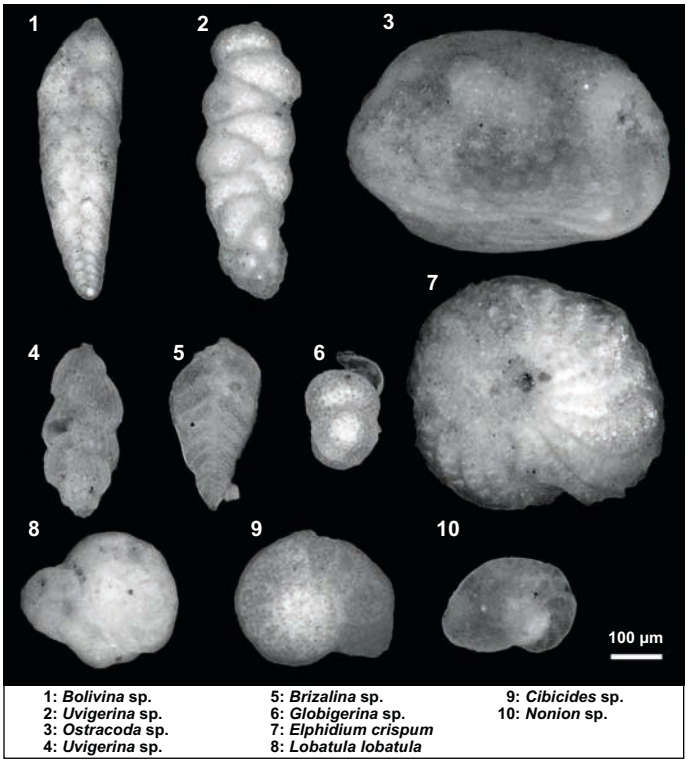

Fig. 14. Scanning electron microscope photos of selected foraminifera specimens and other microfossils found in samples from vibracore GER 3A.

(ca. 15 %). Again, unit VII material is poorly sorted but reveals two maxima, namely in the clay and coarse silt fractions.

The semi-quantitative evaluation of the microfossil content is depicted in Fig. 13. Studied samples (black and white triangles on the right of the vibracore) are consecutively numbered. Selected foraminifera species and other microfossils typical of vibracore GER 43 are shown in Fig. 14. The microfossil content turned out to be unexpectedly high, including a noticeable amount of non-weathered foraminifera tests. Compared to units VI and VII, both the abundance and diversity of foraminifera species are much higher than in units II and III. Fairly many to great many specimens of *Ammonia* sp., *A. beccarii*, *A. tepida*, *Bolivina* sp., *Brizalina* sp., *Bulimina* sp., *Cibicides* sp. and *C. refulgens* were encountered in units VI and VII, while sediments of units II and III only contain a few of these species. In contrast, specimens of *Elphidium* sp., *E. advenum*, *E. crispum*, *Globigerinella* sp., *Lagena* sp., *Lenticulina* sp., *Lobatula lobatula*, *Melonis* sp., *Neoconorbina* sp., *Rectuvigerina* sp., *Rosalina* sp., *Textularia* sp. and *Uvigerina* sp. are almost exclusively associated with sediments of sandy units II and III. Comparing the results of microfossil analyses in the two vibracores studied, the diversity of foraminifera in vibracore GER 3A is lower than the one found for vibracore GER 4A drilled in the river mouth area (Fig. 7). Especially those species (e.g., *Amphistegina lobifera*, *Peneroplis* sp. and *P. pertusus*) that

Table 2. AMS Radiocarbon dating results of samples from vibracore GER 4A. Note: Lab. No. – laboratory number, CEZ – Curt-Engelhorn-Zentrum für Archäometrie, Mannheim, Germany, b.s. – below ground surface, a.s.l. – above sea level, unit – stratigraphic unit, 1σ max, min (cal BC/AD) – calibrated ages, 1σ range, 2σ max; min (cal BC/AD) – calibrated ages, 2σ range. Calibration based on Calib Rev 7.1 with IntCal 13 dataset (Reimer et al. 2013).

Sample	Lab. No. (CEZ)	Depth (m b.s.)	Depth (m a.s.l.)	Sample description	^{14}C Age (BP)	δ^{13}C (‰)	1σ max; min (cal BC/AD)	2σ max; min (cal BC/AD)
GER 4A/19 HR 2.23	26530	2.23	–0.63	wood remains	93 ± 23	–24.9	cal AD 1696-1917	cal AD 1691-1922
GER 4A/33 PR 3.88	26533	3.88	–2.28	plant remains	2660 ± 30	–32.1	cal BC 831-801	cal BC 895-795
GER 4A/42 PR 5.43	26465	5.43	–3.83	plant remains	5199 ± 32	–27.5	cal BC 4039-3971	cal BC 4050-3957
GER 4A/50 PR 6.65	26466	6.65	–5.05	plant remains	42330 ± 730	–29.5	cal BC 44311-43010	cal BC 45123-42372
GER 4A/55 PR 7.59	26467	7.59	–5.99	plant remains	5554 ± 37	–38.1	cal BC 4446-4354	cal BC 4455-4343
GER 4A/71 PR 9.81	26468	9.81	–8.21	plant remains	6633 ± 37	–33.7	cal BC 5619-5543	cal BC 5627-5494

Note: Lab. No. – laboratory number; CEZ – Curt-Engelhorn-Zentrum fur Archaometrie, Mannheim, Germany; b.s. – below ground surface; a.s.l. above sea level; 1σ max, min (cal BC/AD) – calibrated ages, 1σ range; 2σ max, min (cal BC/AD) – calibrated ages, 2σ range. Calibration based on Calib Rev 7.1 with IntCal 13 dataset (Reimer et al 2013).

predominantly occur in the upper part of vibracore GER 4A, starting at ca. 1.90 m b.s. (*4.09 m a.s.l.*) up to present surface, were not found in vibraore GER 3A.

4.3 *Geochronology*

Six samples were retrieved from vibracore GER 4A for ^{14}C AMS radiocarbon dating in order to establish a local event-geochronology for the Geropotamos River study area. Five samples consisted of undetermined plant remains; one sample was made out of wood. Conventional radiocarbon ages were calibrated using the Calib 7.10 software. Radiocarbon dating results are summarised in Table 2. Sample GER 4A/50 PR 6.65 turned out to be pre-Holocene in age attesting strong reworking processes. Age-depth relations of dated samples from core GER 4A (and an age inferred by the first occurrence of *Amphistegina lobiferea*, an invasive foraminifera species) are depicted in Fig. 15 together with results of similar investigations undertaken by Werner et al. (2018b) to the west of Rethymnon and by Lespez et al. (2003) near Malia.

5 *Discussion*

5.1 *Sedimentary facies and palaeoenvironmental evolution*

Based on multi-proxy analyses results, we are able to discriminate between six sedimentary facies for the Geropotamos River study site (Fig. 16). These facies were used to reconstruct palaeoenvironmental changes at the Geropotamos River mouth area and a valley section further inland.

5.1.1 *The Geropotamos River mouth area*

The lower part of sediment core GER 4A is characterised by predominantly low-energy, fine-grained clay and silt (unit I). The mean frequency distribution revealed also a varying minor sand

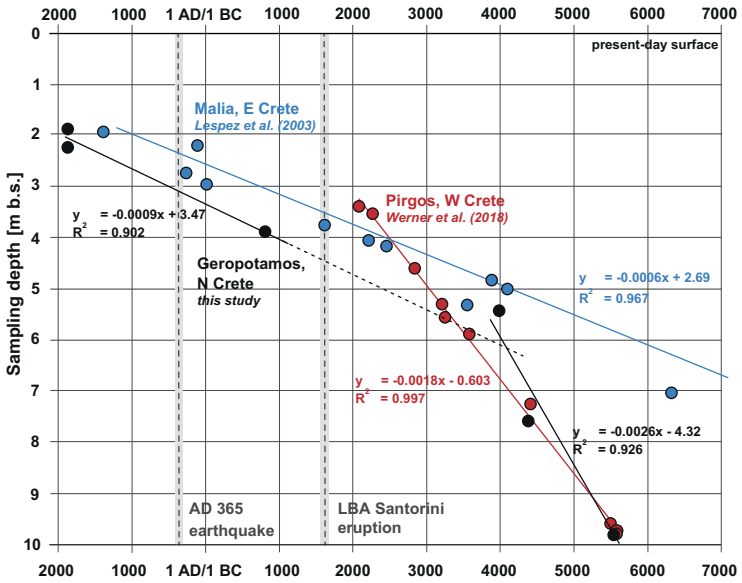

Fig. 15. Age–depth relations reconstructed for the Geropotamos River study site, northern Crete, (this study) compared to age-depth relations for the Pelekanos site near Pirgos, western Crete (Werner et al. 2018b), and Malia, eastern Crete (Lespez et al. 2003, radiocarbon data recalibrated). The vertical dashed lines depict the timeframe of the LBA Santorini (according to Friedrich et al. 2006: 1621–1605 cal BC, 1σ) and the AD 365 tsunami events. The Geropotamos River trend line shows a strong bend where the large hiatus in core GER 4A was found. See text and Fig. 16 for further explanations.

content. In general, the foraminifera abundance and diversity, aside from a high background signal of bedrock-related species (such as *Bolivina* sp., *Brizalina* sp., *Bulimina* sp., *Cibicides* sp., and *Globigerina* sp., see Drinia et al. 2008) is not very high in unit I deposit. However, in comparison to other units, the foraminiferal assemblage of unit I shows an increased abundance of stress tolerating foraminifera species (e.g. *Ammonia tepida* or *Haynesina depressula*) that are typical inhabitants of brackish/lagoonal environments (Murray 2006, Avnaim-Katav et al. 2013). The foraminifera signature includes several tests of species preferring shallow marine habitats (*Ammonia beccarii*, *Elphidium* sp., and *Lenticulina* sp.), indicating a sporadic saltwater influence. Considering the foraminiferal assemblage and the sedimentary characteristics, unit I deposits can be associated with a brackish, more or less sheltered, lagoonal depositional environment. Lagoonal conditions were most probably influenced by the Geropotamos River. It must be noted, that lagoonal deposits of unit I do not include many ostracods and embedded plant remains, as it was described for other lagoonal deposits found at the northern coast of Crete (Bottema & Sarpaki 2003, Werner et al. 2018b). This may be explained by the stronger fluvial influence in this study area.

Fine-grained sediments of unit IV show similar sedimentological and microfossil signals as described for unit I. The foraminiferal signature still gives evidence of a brackish environment with sporadic saltwater influence, however with a weaker signal. The reddish-brown sediment colour is most probably related to increased fluvial input of terrestrial material originating from

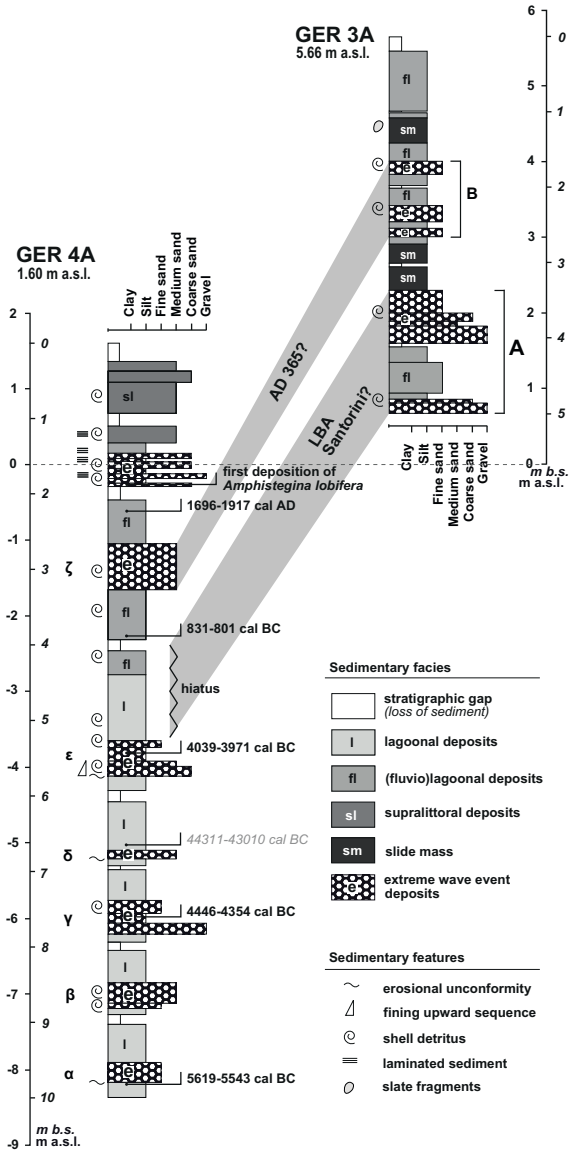

Fig. 16. Vibracore transect showing stratigraphic logs of sediment cores GER 4A and GER 3A. Extreme wave event (EWE) deposits identified in core GER 4A are labelled with Greek letters α to ζ. The uppermost littoral sequence is strongly affected by storm influence. Based on local age-depth relations (Fig. 15), the major hiatus in mid-core position of core GER 4A is suggested to represent the LBA Santorini tsunami event, and event ζ may reflect the AD 365 tsunami event. Candidate layers of the LBA Santorini and the AD 365 tsunamis were also found in core GER 3A drilled on an inactive external bank of the Geropotamos River ca. 1 km inland. For locations of vibracoring sites see Fig. 1, for radiocarbon ages see Table 2. See text and Fig. 15 for further explanations.

the catchment area. Thus, unit IV can be associated with (fluvio-)lagoonal sediments similar to unit I but with an increased fluvial input.

At the present Geropotamos River mouth position, a long-existing (fluvio-)lagoon-type environment left a homogenous sequence that reaches up to 1.90 m b.s. (-0.30 m b.s.l.). Considering the Holocene sea level development, the position of the former coastline must have been situated further in the north of the study area. However, the (fluvio-)lagoonal sequence is interrupted by six sand-dominated intercalations, testifying to high-energy water inflow into a quiet-reach environment. Intercalated high-energy sand layers are characterised by a mixed foraminiferal assemblage with a strongly increased abundance of shallow marine to fully marine foraminifera species. Concerning their preferred habitats, the latter strongly differ from those species found in lagoonal muds. The input of poorly sorted allochthonous marine sand layers and the input of displaced and transported foraminifera species indicate a high-energy turbulent water inflow from the sea side within the course of an extreme wave event (EWE). Because of the overall geomorphological setting and the position of the vibracoring site close to the present shore, it is difficult to clearly assign these layers to storm or tsunami influence – a subject that is later discussed in more detail. Nonetheless, EWE influence was of strictly temporary nature and, as shown by foraminiferal and grain size data, the pre-existing lagoonal environment completely recovered anytime soon after an EWE took place. In Fig. 15 the identified six EWE layers are labelled with Greek letters α to ζ from older to younger respectively.

From 1.90 m b.s. (-0.30 m b.s.l.) to the present surface, a (supra-)littoral sequence follows, consisting almost exclusively of sand and showing an increased Ca/Fe ratio. Although the Ca/Fe ratio was successfully used as a proxy in coastal research in recent studies (for an overview see Chagué-Goff et al. 2010, 2017), there is no reliable trend for the river mouth area, except for the uppermost littoral sequence. The littoral sequence is also characterised by detailed layering associated with all-day littoral dynamics, including sorting and layering of sediments (up to coarse sand) and multiple washover dynamics. Considering the geomorphological setting of vibracore GER 4A, drilled in the landward distal part of a washover fan ca. 50 m south of present-day's beach ridge, it may be speculated that these features are caused by storm influence from the Cretan Sea. The occurrence of *Amphistegina lobifera* at ca. 1.20 m b.s. (0.4 m a.s.l.), an alien species that reached the eastern Mediterranean by opening the Suez channel in AD 1869 (Triantaphyllou et al. 2009), may emphasise reworking processes of the littoral facies during the past 150 or so years.

Based on geochronological data (Fig. 16 and Table 2), we identified a major hiatus between sample GER 4A/33 at 3.88 m b.s. (-2.28 m b.s.l.) and sample GER 4A/42 at 5.43 m b.s. (-3.83 m a.s.l.). The lower part of the sediment core is mid-Holocene in age with high sedimentation rates similar to those found for a lagoonal environment investigated west of Rethymnon (see Werner et al. 2018b), in contrast, the upper part of the core documents the past 2000 or so years. The hiatus is documented in Fig. 15 (dashed black line) starting at a sharp bend in the composite age-depth-relation trend line (see section 5.3).

5.1.2 *Inactive external bank of Geropotamos River further inland*

In this study, we focus on the identification of the impact of potential EWE and their flow dynamics in interaction with the Geropotamos River valley. At the river mouth area, we

detected a (fluvio-)lagoon-type sequence, that was repeatedly affected by marine EWE (α to ζ). In the following, we discuss the question, if one of the EWE has intruded into the Geropotamos River valley and left traces further upstream.

The sedimentary record of core GER 3A is, similar to core GER 4A, characterised by several coarse-grained high-energy layers (units II and III) showing a change in depositional energy in comparison to the over- and underlying fine-grained strata. Poorly sorted unit II and III deposits show a mixture of different grain-sizes varying from coarse silt to coarse sand and gravel. These layers are also related to an increased calcium content that may indicate increased input of biogenic marine carbonate such as marine micro- and macrofauna shells (Vött et al. 2015, Chagué-Goff et al. 2010, 2017), this is corroborated by the results of the microfossil analyses. In general, both abundance and diversity are unexpectedly high with regard to the inland position and overall geomorphological setting of the site. Compared to the over-and underlying strata, the high-energy sand layers show increased abundance and biodiversity of foraminifera. Units II and III show similar marine characteristics as were found for EWE layers in GER 4A in the river mouth area. There are many foraminifera species found both in EWE candidate layers and unit II and III deposits with maximum abundance and diversity at the further landward site GER 3A (Figs 7 and 13). However, from those species almost exclusively restricted to EWE candidate layers at the river mouth, the following species were also exclusively found associated with unit II and III deposits: *Elphidium crispum, Quinqueloculina sp., Rosalina sp.* This may indicate a genetic correlation between EWE impact at the present river mouth and high-energy flow deposits c. 1 km inland (Figs 7 and 13).

However, because of the overall strong foraminiferal fingerprint in vibracore GER 3A, it is difficult to discriminate between marine foraminifera entrained by EWE and the microfossil signal originated from reworked local foraminifera-bearing bedrock sequences. Drinia et al. (2008) investigated benthic foraminifera assemblages in Pliocene marine deposits in the Ierapetra Basin, southeastern Crete, as a base to reconstruct sedimentary environments. This study yielded species such as *Bolivina* sp., *Cibicides* sp., *Lagena* sp., *Lenticulina* sp., *Textularia* sp., and *Uvigerina* sp. to be representative for Pliocene marine deposits. These species were also encountered in high numbers, often in good preservation conditions, in the high-energy sand layers of GER 3A. However, we also found foraminifera species that are not described from Pliocene bedrock units (Drinia et al. 2008), such as *Ammonia* sp., *A. tepida*, *Elphidium crispum*, *Haynesina depressula*, *Quinqueloculina* sp., and *Rosalina* sp. All of them were found more or less exclusively, or with an increasing abundance, associated with EWE candidate layers of vibracore GER 4A at the present river mouth. Based on this assessment, we suppose that the foraminifera signatures along the Geropotamos River bear a strong bedrock signal consisting predominantly of Tertiary marine specimens. Nevertheless, it seems as if there are several species, such as *Ammonia beccarii*, *A. tepida*, and *Haynesina depressula* that were encountered in the (fluvio-)lagoonal sequence found at the present river mouth and in unit I and II layers of GER 3A ca. 1 km inland in a presently inactive external bank position. So, the identification of marine high-energy sand layers and their foraminiferal assemblage may reveal a genetic correlation between EWE impact at the present river mouth area and ca. 1 km inland and may indicate Holocene marine flooding from the Cretan Sea. We therefore interpret unit

II and III deposits of GER 3A as EWE candidate layers. The upper 1.2 m of vibracore GER 4A contain a high quantity of *Amphistegina lobifera*, but this species was not encountered in EWE candidate layers of GER 3A. Consequently, the EWE layers must have been deposited before AD 1869, when the alien species *Amphistegina lobifera* began settling Mediterranean environments due to the opening of the Suez Canal. Additionally, EWE candidate layers do not contain any typical foraminifera species from the littoral zone, such as *Peneroplis* sp. and *Peneroplis pertusus* which are often associated with carbonate-rich sandy beach sediments (Murray 2006, Avnaim-Katav et al., 2013) and were encountered in the upper part of vibracore GER 4A. This also suggests the deposition of EWE candidate layers before the development of the littoral sequence at the present river moth area took place.

Besides the high-energy marine sand layers, the stratigraphic record of GER 3A is dominated by fine-grained fluvial and colluvial deposits (unit VI). The two reddish-brown coloured clay- and silt-dominated unit VII layers are in strong contrast to the under- and overlying strata: The lower unit VII is several decimetres thick whereas the unit VII layer in the upper part of the core shows is slightly thinner, both layers are situated directly on top of an EWE candidate layer. Unit VII deposits are also characterized by high contents of slate and other crystalline bedrock material which make up the valley flanks right seaward of the vibracoring site. Therefore, we interpret unit VII layers as slide mass material from the surrounding valley flanks. The upper unit VIII is subject to present weathering and soil forming processes.

With regard to the geomorphological background, the foraminiferal assemblage, grain size data, and the overall setting of this study area, we interpret the stratigraphic record of vibracore GER 3A as holding the signature of two individual EWE layers from the seaside. The lower EWE layer comprises several unit II and III deposits, reflecting at least two wave pulses and ends up with deposits originating from a slide mass (unit VII). The upper EWE candidate also shows several subsections of unit II, supporting multiple pulses and ends up with a sequence of fluvial deposits and another subsequent slide mass.

5.2 *Origin of the EWE layers*

Searching for the potential origin of EWE layers in the Geropotamos River area, both extreme storm surges and tsunamis must be taken in account. Tsunamites and tempestites are, on a global scale, very similar in their sedimentological characteristics (e.g. Dominey-Howes et al. 2006, Bahlburg & Weiss 2007, Switzer & Jones 2008, Smedile et al. 2011, Rodríguez-Ramírez et al. 2016, Röbke & Vött 2017) and cannot be differentiated easily based on sedimentary features alone. The overall geographical constellation as well as the dominating wind and wave climate and local to regional tectonics have also to be taken into consideration. Especially in the Mediterranean, tsunamis and palaeotsunamis play an essential role in understanding Holocene coastal sedimentary records. They are, in historical times for which numerous accounts on tsunamis exist, much more deadly and costly than storms. In contrast, high-magnitude storms play a subordinate role in the shaping of Mediterranean coastline. So far, the number of regional- and supra-regional-scale tsunamis known and identified by geological evidence is by far larger that the number of storms. The latter have mostly remained on a purely local level. For more details on the role of storms and tsunamis in the Mediterranean, see Vött et al. (2018a, 2018b).

In general, storm surges and tsunamis may be associated with the input of coarse-grained allochthonous sand and gravel in sheltered low-energy sediment environments such as lagoons, back beach swamps or harbour basins (Vött & May 2009, Vött et al. 2018b). In contrast to long-waved tsunamis, storm waves often leave thin-layered deposits and comprise nearshore material, for example beach and nearshore sands. In contrast, tsunami deposits may comprise a wide range of source material ranging from open marine, shelf, littoral and even terrestrial environments (Switzer & Jones 2008, Röbke & Vött 2017). After the 2004 Indian Ocean tsunami and the 2011 Tōhoku-oki tsunami, numerous studies on tsunami deposits characterisation have been carried out (e.g. Bahlburg & Weiss 2007, Choowong et al. 2008, Goto et al. 2011, Richmond et al. 2012). Several depositional signatures such as a long distance landward transport of sediment often accompanied by a landward thinning were identified as typical of tsunami influence (Bahlburg & Weiss 2007, Richmond et al. 2012). Affected by different flow dynamics of the water masses during different stages of inundation and backflow (Choowong et al. 2008), tsunamites are often characterised by fining upward sequences of grain sizes, a broad spectrum of different grain sizes, bi- or multi-modal deposits, rip-up clasts, basal erosional unconformities and poor sorting (e.g., Dominey-Howes 2004, Dominey-Howes et al. 2006, Bahlburg & Weiss 2007, Switzer & Jones 2008, Goto et al. 2011, Richmond et al. 2012, Röbke & Vött 2017). As a tool to identify the input of marine sediment, Chagué-Goff et al. (2010, 2017) applied geochemical analyses and successfully used calcium and strontium signals to identify tsunami signatures. Also, the evaluation of the foraminiferal content has been used as a tool to indicate general palaeoenvironmental changes and to identify tsunami deposits (Dominey-Howes et al. 2006, Pilarczyk et al. 2014). Several studies on Mediterranean palaeotsunamis proved a mixed assemblage of foraminifera from different ecological habitats and preservation states to be characteristic for tsunami deposits (Reinhardt et al. 1994, Goodman et al. 2008, Hadler et al. 2013, Mathes-Schmidt et al. 2013, Fischer et al. 2016, Finkler et al. 2018a, 2018b, Werner et al. 2018a, 2018b). However, tsunami-influenced foraminiferal assemblages differ from study site to study site and are strongly affected by local geomorphological and bathymetrical conditions. Most reliable arguments for tsunami influence are displaced and transported species, for example, open marine to shallow marine species found in protected lagoonal or marsh settings (Mamo et al. 2009, Pilarczyk et al. 2014).

In the Mediterranean, numerous palaeotsunamites have already been detected in different sedimentary archives, for example along the coasts of the Aegean, Ionian, and Adriatic seas and along the northeastern and southwestern coasts of Crete (e.g., Pirazzoli et al. 1992, De Martini et al. 2003, Bruins et al. 2008, Vött et al. 2009, 2011a, 2011b, 2014, 2015, Reicherter et al. 2010, Kortekaas et al. 2011, Mastronuzzi & Sansò 2012, Koster et al. 2015, Willershäuser et al. 2015, Quintela et al. 2016, Werner et al. 2018a, 2018b).

Transferring the described signatures found typical of Mediterranean tsunamis to the Geropotamos River mouth area, the following analogies can be found: EWE layers are poorly sorted, contain a broad spectrum of different grain sizes and shell fragments, show a fining upward sequence (layer ε), are bi- to multi-modal, contain a mixed foraminiferal signature, and show erosional unconformities towards the underlying strata. However, the Ca/Fe ratio of sediments from the study area do not depict a clear allochthonous signal most probably due to masking effects by local bedrock units.

We also identified EWE layers in the sedimentary record of the landward Geropotamos valley study area. Here, they also appeared poorly sorted, contain a broad spectrum of different grain sizes as well as shell fragments, contain a strong foraminiferal bedrock signal but also fresh displaced marine species. Finally, EWE layer characteristics are in contrast to the over- and underlying strata. Considering the distance of more than 1 km to the present coast – the palaeoshore line was situated even further seaward than today (see above) – storms as origin for these EWE layers can certainly be excluded. Bound to high-frequency waves, Mediterranean storms do not produce water masses large enough to realize inundation distances that long. A recent geomorphological survey in the neighbouring, funnel shaped Eko creek valley located some 600 meters to the SW of the Geropotamos River mouth, have shown that storm-driven wooden debris and small cobbles were transported maximum 140 m inland during several storm events in 2014. These storm sediments were very thin-layered and patchy. For further discussion of the capacity of storms in the region see Soukissian et al. (2008), Alexandrakis et al. (2013), Ayat (2013), Tsoukala et al. (2016) and Werner et al. (2018b). We conclude, that the geomorphodynamic potential of the EWE candidate layers found at site GER 3A is far beyond what storms can produce in the Cretan Sea and in the Mediterranean. Consequently, it can be inferred as a reverse conclusion that corresponding EWE layers at the river mouth are of tsunami-related origin as well.

5.3 *Tsunami inundation along river valleys*

Rivers usually serve as drainage for surface waters. However, river mouth areas along the coasts are also prone to tsunami penetration as was observed by recent tsunami events of 2004 and 2011 (Adityawan et al. 2012, Tanaka et al. 2012, 2014, Tolkova & Tanaka 2016). During the 2011 Tōhoko-oki tsunami, tsunami waves entered the Kitakami River and propagated up to 17 km inland causing widespread inundation along the riverbank (Tolkova & Tanaka 2016). Tsunami wave propagation along large rivers is characterised by reduced friction and waves maintain their energy far upstream and are able to cause massive landward damage (Tanaka et al. 2012). The river mouth geometry and geomorphological features such as sand spits or jetties directly influence wave propagation distances (Adityawan et al. 2012, Tanaka et al. 2012). Other important factors are meanders, water depth, bottom friction and the river bed slope (Tanaka et al. 2012, Chanson & Lublin 2013). Based on laboratory experiments and a theoretical approach, Tsuji et al. (1991) suggested that the height of a tsunami in rivers may be amplified by a factor of 1.5. Furthermore, tsunami wave propagation in rivers was found to be associated with strong sediment mixing and massive input of terrestrial sediments (Chanson & Lublin 2013). In the central part of the Gulf of Cadiz, Morales et al. (2008) identified five different tsunami layers in the sedimentary record of the Huelva Estuary that could be traced upstream over a distance of ten kilometres. Viana-Baptista et al. (2006) calculated tsunami propagation models along the Tagus Estuary of Lisbon, Portugal, that are consistent with geomorphological and sedimentological field evidence and underline the risk of tsunami propagation in rivers and estuaries. In Greece, studies carried out by Ntageretzis et al. (2015b) in a valley to the northwest of Neapoli Vion, Vatika Bay, found tsunami evidence up to at least 400 m inland. The valley, incised into older lithified Pleistocene fans and marine terraces, produced funnelling and acceleration effects that let tsunami waters intrude far inland.

5.4 *Reconstruction of Geropotamos valley flow dynamics*

Considering tsunami-related flooding of the Geropotamos River valley is only plausible if the valley morphology is taken into account. As shown above, the latter may have a significant influence on the tsunami propagation upstream (Tanaka et al. 2012, 2014). The Geropotamos River mouth area is triangle-type, funnel-shaped, non-blocked, and would to catch large water masses of long-wave tsunami waters. The subsequent narrow and incised valley would then have strongly channelled and accelerated intruding water masses towards inland.

We further suppose that channelled water inflow produced strong undercut in outer/external bank positions. The GER 3A sedimentary record shows several sections of unit VII deposits, which are characterized by slate and other crystalline bedrock material which make up the valley flanks right seaward of the vibracoring site. We interpret these units as due to mass wasting triggered by strong undercut processes. It is furthermore striking that unit VII deposits were found directly on top of EWE candidate (units II) so that one might assume that tsunami landfall itself (rather than normal river dynamics) and following inland channelization of waters is the major cause for these slide masses retrieved in core GER 3A.

5.5 *Age-depth relations*

The study area is located to the east of the region of Crete that is known to have experienced co-seismic uplift during the AD 365 earthquake. In the frame of their study at Pirgos, located to the west of Rethymnon, Werner et al. (2018b) found sedimentary evidence of coseismic uplift in the range of 1.6 m during the AD 365 event. We compared age-depth trend lines achieved for selected sites along the north coast of Crete, namely the Pirgos site (Werner et al. 2018b), the area around Malia (Lespez et al. 2003), and the Geropotamos River study site (Fig. 15). The older part of the trend line obtained for the Geropotamos River study is almost identical with the general trend line obtained for the Pelekanos site near Pirgos, west of Rethymnon. Starting with a strong bend through the large hiatus in core GER 4A somewhere between ca. 4 m and 5.20 m b.s., however, the trend line subsequently flattens and runs parallel to the line obtained for the Malia study site until more recent times. This general change in slope of the Geropotamos River trend line apparently indicates a change in the subsidence rate of the site (see above), in any case a considerable rise of the relative sea level. However there are several possibilities to explain and date the hiatus itself. First, it may be speculated that the hiatus was caused by strong coseismic uplift at some point in time between the 5th and the 1st mill. BC by which considerably reduced the accommodation space. Second, erosive processes may have removed large parts of the sedimentary record. As we are in the distal part of the fluvial system, namely at the river mouth, relevant erosion by the river system itself seems rather improbable. However, one may consider erosion by tremendous EWE from the seaside, possibly by the tsunami waves in conjunction with the LBA Santorini eruption that hit the north coast of Crete (Lespez et al. 2003, Bruins et al. 2008, Werner et al. 2018b).

Based on the younger part of the Geropotamos River trend line, we approximated the depth where the sediments of the AD 365 earthquake and tsunami event can be expected as ca. 3 m b.s. (Fig. 15). This is exactly the depth where the sedimentary record of core GER 4A shows

EWE-related coarse-grained unit V deposits (Figs 5, 6, 7, and 15). We therefore hypothesize that EWE deposit ζ in core GER 4A is a candidate deposit of the AD 365 tsunami. Considering that the youngest tsunamites recorded in the Pirgos archive to west of Rethymnon are the LBA Santorini event and the AD 365 event (Werner et al. 2018b), we further hypothesize that the two major potential tsunamites A and B identified in core GER 3A may represent these two events (Fig. 16). On this speculative base, A would thus be consistent with the LBA Santorini event deposit and B would be consistent with the AD 365 tsunamite. However, to further study this question, more precise dating of the EWE deposits recovered from site GER 3A would be required. In this respect, the most promising approach is using OSL dating techniques.

Our evidence supports the suggestion, that the Geropotamos River mouth area is a good archive for mid-Holocene EWE events. For a period of minimum 1700 or so years from the midst of the 6th to the end of the 5th mill. BC, we found sedimentary and microfossil evidence of five EWE. In contrast, the Pirgos sedimentary archive (Werner et al. 2018b) has recorded three EWE for the time period between the midst of the 4th and the end of the 3rd mill. BC. Finally, as already discussed above, we suggest that both the LBA Santorini and the AD 365 tsunami events are recorded in both study areas. Overall, the event history based on our analyses indicates 10 EWE (Werner et al. 2018b and this study), of them clearly defined as tsunamis, during the past ca. 7500 years. This results in a statistical average recurrence interval of ca. 750 years for major EWE in this area. This is consistent with the assessment of Shaw et al. (2008) and Shaw (2012), who stated that tsunami events of the AD 365-type magnitude may occur every 800 years along the Hellenic subduction zone.

6 *Conclusions*

The Geropotamos River mouth sedimentary archive revealed specific signatures of repeated EWE influence since the mid-Holocene. The EWE signatures are coarse-grained, sand-dominated layers of few decimetres thickness with a shallow marine to marine foraminiferal background and intersect more or less homogeneous silt-dominated (fluvio-)lagoonal muds making up major parts of the local sedimentary record.

Based on grain size and microfossil evidence, at least during some EWE events, inundation reached minimum 1 km inland, leaving EWE signatures in a presently inactive external bank position of the Geropotamos River and triggering mass failures.

Signatures reliably assigned to storm influence are restricted to the uppermost 1.9 m of the sedimentary record in the Geropotamos River mouth area, when the lagoonal environment had already stopped to exist and littoral processes have dominated the vibracoring site. Obviously, storm influence seems to be mostly restricted to the (supra-)littoral zone itself. The appearance of *Amphistegina lobifera*, an alien species that spread with the opening of the Suez Canal in AD 1869 through the Mediterranean basin, suggests a depositional period of ca. 150 years for the uppermost 1.20 m of the littoral facies.

We hypothesize that the major hiatus found in the Geropotamos River mouth archive may be related to erosional effects of the LBA Santorini tsunami known to have severely hit the north coast of Crete and/or may reflect changes in the subsidence rate and the local accommodation

space architecture. The youngest EWE signal – based on specific age-depth relations – appears to have been caused by the AD 365 tsunami event. Candidate deposits for both tsunami events were identified ca. 1 km further inland documenting channelling and acceleration effects of intruding water masses in the narrow and steeply incised Geropotamos River valley in an upstream direction. However, further geochronological studies based on OSL dating are required to render reliable age control for these deposits.

Together with the Pirgos sedimentary archive (Werner et al. 2018b), the Geropotamos River valley record revealed evidence of ten major EWE that hit the north coast of Crete during the past 7500 or so years leading to a statistical recurrence interval of ca. 750 years for large EWE impacts. This is consistent with statistical recurrence intervals for major tsunamis based on seismological studies (Shaw et al. 2008, Shaw 2012) and underlines the generally high tsunami hazard of the region.

Acknowledgements

We are kindly indebted to the Ephorate of Antiquities of Rethymnon, Hellenic Ministry of Culture, for their precious help and support during field campaigns. Geological work permits were issued by the Institute for Geology and Mineral Exploration (IGME, Athens) which is gratefully acknowledged. We also thank M. Drusenheimer and S. Ertel for their effort especially with microfossil samples. This study was founded by the German Research Foundation (DFG, Germany) with grants to K. Reicherter (RE 1361/19-1) and A. Vött (VO 938/12-1).

References

Adityawan, M. B., Roh, M., Tanaka, H., Mano, A. & Udo, K. (2012): Investigation of tsunami propagation characteristics in river and on land induced by The Great East Japan Earthquake 2011. – Journal of Earthquake and Tsunami **6** (3): 1–22, doi: 10.1142/S1793431112500339.

Alexandrakis, G., Poulos, S., Petrakis, S. & Collins, M. (2011): The development of a Beach Vulnerability Index (BVI) for the assessment of erosion in the case of the North Cretan Coast (Aegean Sea). – Hellenic Journal of Geosciences **45:** 11–22.

Ambraseys, N. (2009): Earthquakes in the Mediterranean and Middle East. A multidisciplinary study of seismicity up to 1900. – Cambridge University Press, 968 pp., Cambridge.

Angelier, J., Lybéris, N., Le Pichon, X., Barrier, E. & Huchon, P. (1982): The Tectonic Development of the Hellenic Arc and the Sea of Crete: A Synthesis. – Tectonophysics **86:** 159–169.

Avnaim-Katav, S., Almogi-Labin, A., Sandler, A. & Sivan, D. (2013): Benthic foraminifera as palaeoenvironmental indicators during the last million years in the eastern Mediterranean inner shelf. – Paleogeography, Palaeoclimatology, Palaeoecology **386:** 512–530, doi: 10.1016/j.palaeo.2013.06.019.

Ayat, B. (2013): Wave power atlas of Eastern Mediterranean and Aegean seas. – Energy **54:** 251–262.

Bahlburg, H. & Weiss, R. (2007): Sedimentology of the December 26, 2004, Sumatra tsunami deposits in eastern India (Tamil Nadu) and Kenya. – International Journal of Earth Sciences **96** (6): 1195–1209.

Bohnhoff, M., Makris, J., Papanikolaou, D. & Stavrakakis, G. (2001): Crustal investigation of the Hellenic subduction zone using wide aperture seismic data. – Tectonophysics **343:** 239–262.

Bony, G., Marriner, N., Morhange, C., Kaniewski, D. & Perinçek, D. (2012): A high-energy deposit in the Byzantine harbour of Yenikapı, Istanbul (Turkey). – Quaternary International **266:** 117–130.

Bottema, S. & Sarpaki, A. (2003): Environmental changes in Crete: a 9000-year record of Holocene vegetation history and the effect of the Santorini eruption. – The Holocene **13** (5): 733–749, doi: 10.1191/0959683603hl659rp.

Boulton, S. J. & Whitworth, M. R. (2017): Block and boulder accumulations on the southern coast of Crete (Greece): evidence for the 365 CE tsunami in the Eastern Mediterranean. – Geological Society, London, Special Publications **456:** SP456–4.

Bruins, H. J., MacGillivray, J. A., Synolakis, C. E., Benjamini, C., Keller, J., Kisch, H. J., Klügel, A. & van der Plicht, J. (2008): Geoarchaeological tsunami deposits at Palaikastro (Crete) and the Late Minoan IA eruption of Santorini. – Journal of Archaeological Science **35** (1): 191–212, doi: 10.1016/j.jas.2007.08.017.

Caputo, R., Catalano, S., Monaco, C., Romagnoli, G., Tortorici, G. & Tortorici, L. (2010): Active faulting on the island of Crete (Greece). – Geophysical Journal International **183:** 111–126.

Chaguéé-Goff, C. (2010): Chemical signatures of palaeotsunamis: A forgotten proxy? – Marine Geology **271** (1–2): 67–71.

Chaguéé-Goff, C., Szczuciński, W. & Shinozaki, T. (2017): Applications of geochemistry in tsunami research: A revive. – Earth-Science Reviews **165:** 203–244.

Chanson, H. & Lubin, P. (2013): Mixing and Sediment Processes induced by Tsunamis propagating Upriver. – In: Tsunamis: Economic Impact, Disaster Management and Future Challenges. – Nova Science Publishers, 65–102, Hauppauge NY, USA.

Choowong, M., Murakoshi, N., Hisada, K., Charoentitirat, T., Charusiri, P., Phantuwongraj, S., Wongkok, P., Choowong, A., Subsayjun, R., Chutakositkanon, V., Jankaew, K. & Kanjanapayont, P. (2008): Flow conditions of the 2004 Indian Ocean tsunami in Thailand, inferred from capping bedforms and sedimentary structures. – Terra Nova **20:** 141–149.

Cimerman, F. & Langer, M. R. (1991): Mediterranean Foraminifera. – Slovenska Akademija Znanosti, 118 pp., Ljubljana.

De Martini, P. M., Burrato, P., Pantosti, D., Maramai, A., Graziani, L. & Abramson, H. (2003): Identification of tsunami deposits and liquefaction features in the Gargano area (Italy): paleoseismological implication. – Annals of Geophysics **46** (5): 883–902.

De Martini, P. M., Barbano, M. S., Smedile, A., Gerardi, F., Pantosti, D., Del Carlo, P. & Pirrotta, C. (2010): A unique 4000 year long geological record of multiple tsunami inundations in the Augusta Bay (eastern Sicily, Italy). – Marine Geology **276** (1–4): 42–57.

DIN/EN ISO 11277 (2002): Bodenbeschaffenheit – Bestimmung der Partikelgrößenverteilung in Mineralböden – Verfahren mittels Siebung und Sedimentation. ISO 11277: 1998 and ISO 11277, Corrigendum 1. – Beuth Verlag GmbH, Berlin.

Dominey-Howes, D. (2004): A re-analysis of the Late Bronze Age eruption and tsunami of Santorini, Greece, and the implications for the volcano-tsunami hazard. – Journal of Volcanology and Geothermal Research **130:** 107–132.

Dominey-Howes, D. T., Humphreys, G. S. & Hesse, P. P. (2006): Tsunami and palaeotsunami depositional signatures and their potential value in understanding the late-Holocene tsunami record. – The Holocene **16** (8): 1095–1107.

Doutsos, T. & Kokkalas, S. (2001): Stress and deformation patterns in the Aegean region. – Journal of Structural Geology **23:** 455–472.

Drinia, H., Antonarakou, A. & Kontakiotis, G. (2008): On the occurrence of early Pliocene marine deposits in the Ierapetra Basin, eastern Crete, Greece. – Bulletin of Geosciences **83** (1): 63–78.

Finkler, C., Fischer, P., Baika, K., Rigakou, D., Metallinou, G., Hadler, H. & Vött, A. (2018a): Tracing the Alkinoos Harbor of ancient Kerkyra, Greece, and reconstructing its paleotsunami history. – Geoarchaeology **33** (1): 24–42, doi: 10.1002/gea.21609.

Finkler, C., Baika, K., Rigakou, D., Metallinou, G., Fischer, P., Hadler, H., Emde, K. & Vött, A. (2018b): Geoarchaeological investigations of a prominent quay wall in ancient Corcyra-Implications for harbour development, palaeoenvironmental changes and tectonic geomorphology of Corfu Island (Ionian Islands, Greece). – Quaternary International **473:** 91–111, doi: 10.1016/j.quaint.2017.05.013.

Fischer, P. Finkler, C., Röbke, B. R., Baika, K., Hadler, H., Willershäuser, T., Rigakou, D., Metallinou, G. & Vött, A. (2016): Impact of Holocene tsunamis detected in lagoonal environments on Corfu (Ionian Islands, Greece) – geomorphological, sedimentary and microfaunal evidence. – Quaternary International **401:** 4–16, doi: 10.1016/j.quaint.2015.07.019.

Flouri, E. T., Kalligeris, N., Alexandrakis, G., Kampanis, N. A. & Synolakis, C. E. (2013): Application of a finite difference computational model to the simulation of earthquake generated tsunamis. – Applied Numerical Mathematics **67:** 111–125.

Font, E., Nascimento, C., Omira, R., Baptista, M. A. & Silva, P. F. (2010): Identification of tsunami-induced deposits using numerical modeling and rock magnetism techniques: A study case of the 1755 Lisbon tsunami in Algarve, Portugal. – Physics of the Earth and Planetary Interiors **182:** 187–198, doi: 10.1016/j.pepi.2010.08.007.

Friedrich, W. L., Kromer, B., Friedrich, M., Heinemeier, J., Pfeiffer, T. & Talamo, S. (2006): Santorini Eruption Radiocarbon Dated to 1627–1600 B. C. – Science **312:** 548, doi: 10.1126/science.1125087.

Galanopoulos, A. G. (1960): Tsunamis observed on the coasts of Greece from antiquity to present time. – Annals of Geophysics **13** (3–4): 369–386.

Gianfreda, F., Mastronuzzi, G. & Sansò, P. (2001): Impact of historical tsunamis on a sandy coastal barrier: an example from the northern Gargano coast, southern Italy. – Natural Hazards and Earth System Science **1** (4): 213–219.

Goodman, B., Reinhardt, E., Dey, Hendrik, Boyce, J., Schwarcz, H., Sahoglu, V., Erkanal, H. & Artzy, M. (2008): Evidence for Holocene marine transgression and shoreline progradation due to barrier development in Iskele, Bay of Izmir, Turkey. – Journal of Coastal Research **24** (5): 1269–1280, doi: 10.2112/06-0811.1.

Goodman-Tchernov, B. N., Dey, H. W., Reinhardt, E. G., McCoy, F. & Mart, Y. (2009): Tsunami waves generated by the Santorini eruption reached Eastern Mediterranean shores. – Geology **37:** 943–946, doi: 10.1130/G25704A.1.

Goto, K., Chagué-Goff, C., Fujino, S., Goff, J., Jaffe, B., Nishimura, Y., Richmond, B., Sugawara, D., Szczuciński, W., Tappin, D. R., Witter, R. C. & Yulianto, E. (2011): New insights of tsunami hazard from the 2011 Tohoku-oki event. – Marine Geology **290:** 46–50, doi: 10.1016/j.margeo.2011.10.004.

Guidoboni, E., Comastri, A. & Traina, G. (1994): Catalogue of Ancient Earthquakes in the Mediterranean up to the 10th Century. – Istituto Nazionale di Geofisica, 504 pp., SGA, Roma.

Hadler, H., Willershäuser, T., Ntageretzis, K., Henning, P. & Vött, A. (2012): Catalogue entries and non-entries of earthquake and tsunami events in the Ionian Sea and the Gulf of Corinth (eastern Mediterranean, Greece) and their interpretation with regard to palaeotsunami research. – In: Vött, A. & Venzke, J. F. (eds): Beiträge der 29. Jahrestagung des Arbeitskreises "Geographie der Meere und Küsten", 28. bis 30. April 2011 in Bremen, Bremer Beiträge zur Geographie und Raumplanung **44:** 1–15.

Hadler, H., Vött, A., Koster, B., Mathes-Schmidt, M., Mattern, T., Ntageretzis, K., Reicherter, K. & Willershäuser, T. (2013): Multiple late-Holocene tsunami landfall in the eastern Gulf of Corinth recorded in the palaeotsunami geoarchive at Lechaion, harbour of ancient Corinth (Peloponnese, Greece). – Zeitschrift für Geomorphologie N. F., Supplementary Issue **57** (4): 139–180, doi: 10.1127/0372-8854/2013/S-00138.

Hadler, H., Baika, K., Pakkanen, J., Evangelistis, D., Fischer, P., Ntageretzis, K., Röbke, B., Willershäuser, T. & Vött, A. (2015): Palaeotsunami impact on the ancient harbour site Kyllini (western Peloponnese, Greece) based on a geomorphological multi-proxy approach. – Zeitschrift für Geomorphologie N. F., Supplementary Issue **59** (4): 7–41, doi: 10.1127/zfg_suppl/2014/S00187.

Hindson, R. A., Andrade, C. & Dawson, A. G. (1996): Sedimentary processes associated with the tsunami generated by the 1755 Lisbon earthquake on the Algarve coast, Portugal. – Physics and Chemistry of the Earth, **21:** 57–63. doi: 10.1016/S0079-1946(97)00010-4.

Hollenstein, C., Müller, M. D., Geiger, A. & Kahle, H.-G. (2008): Crustal motion and deformation in Greece from a decade of GPS measurements, 1993–2003. – Tectonophysics **449:** 17–40.

Institute of Geological and Mining Research (IGMR) (1977): General geological map of Greece. Crete Island. Scale 1:200.000.

Jolivet, L., Goffé, B., Monié, P., Truffert-Luxey, C., Patriat, M. & Bonneau, M. (1996): Miocene detachment in Crete and exhumation P-T-t paths of high-pressure metamorphic rocks. – Tectonics **15** (6): 1129–1153.

Judd, K., Chagué-Goff, C., Goff, J., Gadd, P., Zawadzki, A. & Fierro, D. (2017): Multi-proxy evidence for small historical tsunamis leaving little or no sedimentary record. – Marine Geology **385:** 204–215.

Kelletat, D. (1991): The 1550 BP tectonic event in the Eastern Mediterranean as a basis for assuring the intensity of shore processes. – Zeitschrift für Geomorphologie **81:** 181–194.

Köhn, M. (1929): Korngrößenbestimmung vermittels Pipettanalyse. – Tonindustrie-Zeitung **55:** 729–731.

Kontopoulos, N. & Avramidis, P. (2003): A late Holocene record of environmental changes from the Aliki lagoon, Egion, North Peloponnesus, Greece. – Quaternary International **111** (1): 75–90.

Kortekaas, S., Papadopoulos, G. A., Ganas, A., Cundy, A. B. & Diakantoni, A. (2011): Geological identification of historical tsunamis in the Gulf of Corinth, Central Greece. – Natural Hazards and Earth System Sciences **11** (7): 2029–2041.

Koster, B., Vött, A., Mathes-Schmidt, M. & Reicherter, K. (2015): Geoscientific investigations in search of tsunami deposits in the environs of the Agoulinitsa peatland, Kaiafas Lagoon and Kakovatos (Gulf of Kyparissia, western Peloponnese, Greece). – Zeitschrift für Geomorphologie N. F., Supplementary Issues **59** (4): 125–156, doi: 10.1127/zfg_suppl/2014/S-00192.

Le Pichon, X. & Angelier, J. (1979): The Hellenic arc and trench system: a key to the neotectonic evolution of the eastern Mediterranean area. – Tectonophysics **60** (1): 1–42.

Lespez, L., Dalongeville, R., Pastre, J. F., Darmon, F., Mathieu, R. & Poursoulis, G. (2003): Late-Middle-Holocene palaeo-environmental evolution and coastline changes of Malia (Crete). – The Mediterranean World Environment and History, 439–452, Elsevier, Amsterdam.

Lorito, S., Tiberti, M. M., Basili, R., Piatanesi, A. & Valensise, G. (2008): Earthquake-generated tsunamis in the Mediterranean Sea: Scenarios of potential threats to southern Italy. – Journal of Geophysical Research: Solid Earth **113** (B1: 1–14), doi: 10.1029/2007JB004943.

Mamo, B., Strotz, L. & Dominey-Howes, D. (2009): Tsunami sediments and their foraminiferal assemblages. – Earth Science Reviews **96:** 263–278.

Mason, J., Schneiderwind S., Pallikarakis, A., Wiatr T., Mechernich, S., Papanikolaou, I. & Reicherter, K. (2016): Fault structure and deformation rates at the Lastros-Sfaka Graben, Crete. – Tectonophysics **683:** 216–232.

Mastronuzzi, P. & Sansò, P. (2012): The role of strong earthquakes and tsunami in the Late Holocene evolution of the Fortore River coastal plain (Apulia, Italy): A synthesis. – Geomorphology **138** (1): 89–99.

Mathes-Schmidt, M., Schwarzbauer, J., Papanikolaou, I., Syberberg, F., Thiele, A., Wittkopp, F. & Reicherter, K. (2013): Geochemical and micropalaeontological investigations of tsunamigenic layers along the Thracian Coast (Northern Aegean Sea, Greece). – Zeitschrift für Geomorphologie, N. F., Supplementary Issue **57** (4): 5–27.

May, S. M., Vött, A., Brückner, H. & Smedile, A. (2012): The Gyra washover fan in the Lefkada Lagoon, NW Greece – possible evidence of the 365 AD Crete earthquake and tsunami. – Earth, planets and space **64** (10): 6.

McClusky, S., Balassanian, S., Barka, A., Demir, C., Ergintav, S., Georgiev, I., Gurkan, O., Hamburger, M., Hurst, K., Kahle, H., Kastens, K., Kekelidze, G., King, R., Kotzev, V., Lenk, O., Mahmoud, S., Mishin, A., Nadariya, M., Ouzounis, A., Paradissis, D., Peter, Y., Prilepin, M., Reilinger, R., Sanli, I., Seeger, H., Tealeb, A., Toksöz, M. N. & Veis, G. (2000): Global positioning system constraints on plate kinematics and dynamics in the eastern Mediterranean and Caucasus. – Journal of Geophysical Research: Solid Earth **105:** 5695–5719.

McKenzie, D. (1972): Plate Tectonics of the Mediterranean Region. – Nature **226:** 239–243.

McKenzie, D. (1978): Active tectonics of the Alpine Himalayan Belt, the Aegean Sea and surrounding regions. – Geophysical Journal International **55** (81): 217–254.

Meulenkamp, J. E., van der Zwaan, G. J. & van Wamel, W. A. (1994): On late Miocene to recent vertical motions in the Cretan segment of the Hellenic arc. – Tectonophysics **234:** 53–72.

Morales, J. A., Borrego, J., San Miguel, E. G., López-González, N. & Carro, B. (2008): Sedimentary record of recent tsunamis in the Huelva Estuary (southwestern Spain). – Quaternary Science Reviews **27** (7–8): 734–746.

Mouslopoulou, V., Begg, J., Nicol, A., Oncken, O. & Prior, C. (2015): Formation of Late Quaternary paleoshorelines in Crete, Eastern Mediterranean. – Earth and Planetary Science Letter **431:** 294–307.

Murray, J. W. (2006): Ecology and Application of Benthic Foraminifera. – Cambridge University Press, 426 pp., Cambridge.

Nomikou, P., Hübscher, C., Papanikolaou, D., Farangitakis, G. P., Ruhnaub, M. & Lampridou, D. (2018): Expanding extension, subsidence and lateral segmentation within the Santorini – Amorgos basins during Quaternary: Implications for the 1956 Amorgos events, central – south Aegean Sea, Greece. – Tectonophysics **722:** 138–153.

Ntageretzis, K., Vött, A., Fischer, P., Hadler, H., Emde, K., Röbke, B. R. & Willershäuser, T. (2015a): Palaeotsunami history of the Elos Plain (Evrotas River delta, Peloponnese, Greece). – Zeitschrift für Geomorphologie, Supplementary Issues **59** (4): 253–273.

Ntageretzis, K., Vött, A., Emde, K., Fischer, P., Hadler, H., Röbke, B. R. & Willershäuser, T. (2015b): Palaeotsunami record in near-coast sedimentary archives in southeastern Lakonia (Peloponnese, Greece). – Zeitschrift für Geomorphologie, Supplementary Issues **59** (4): 275–299.

Papadopoulos, G. A. & Chalkis, B. J. (1984): Tsunami observed in Greece and the surrounding area from antiquity up to present times. – Marine Geology **56:** 309–317.

Papadopoulos, G. A., Daskalaki, E., Fokaefs, A. & Giraleas, N. (2007): Tsunami hazard in the Eastern Mediterranean: strong earthquakes and tsunamis in the East Hellenic arc and trench system. – Natural Hazards and Earth System Sciences **7:** 57–64.

Papadopoulos, G. A., Gràcia, E., Urgeles, R., Sallares, V., De Martini, P. M., Pantosti, D., González, M., Yalciner, A. C., Mascle, J., Sakellariou, D., Salamon, A., Tinti, S., Karastathis, V., Fokaefs, A., Camerlenghi, A. Novikova, T. & Papageorgiou, A. (2014): Historical and pre-historical tsunamis in the Mediterranean and its connected seas: Geological signatures, generation mechanisms and coastal impacts. – Marine Geology **354:** 81–109.

Papanikolaou, D. & Vassilakis, E. (2010): Thrust faults and extensional detachment faults in Cretan tectonostratigraphy: implications for Middle Miocene extension. – Tectonophysics **488:** 233–247.

Papazachos, V., Papazachos, B., Papazachou, C. & Papazachou, K. (1997): The earthquakes of Greece. – Editions Ziti, 304 pp., Thessaloniki.

Peterek, A. & Schwarze, J. (2004): Architecture and Late Pliocene to recent evolution of outer-arc basins of Hellenic subduction zone (south-central Crete, Greece). – Journal of Geodynamics **38:** 19–55.

Pilarczyk, J. E., Dura, T., Horton, B. P., Engelhart, S. E., Kemp, A. C. & Sawai, Y. (2014): Microfossils from coastal environments as indicators of paleo-earthquakes, tsunamis and storms. – Returning to the facts. – Palaeogeography, Palaeoclimatology, Palaeoecology **413:** 144–157, doi: 10.1016/j.palaeo.2014.06.033.

Pirazzoli, P. A., Thommeret, J., Thommeret, Y., Laborel, J. & Montaggioni, L. F. (1982): Crustal block-movements from Holocene shorelines: Crete and Antikythira (Greece). – Tectonophysics **86:** 27–43.

Pirazzoli, P. A., Ausseil-Badie, J., Giresse, P., Hadjidaki, E. & Arnold, M. (1992): Historical environmental Changes at Phalasarna harbor, west Crete. – Geoarchaeology **7:** 371–392.

Pirazzoli, P. A., Laborel, J. & Stiros, S. C. (1996): Earthquake clustering in the Eastern Mediterranean during historical times. – Journal of Geophysical Research **101:** 6083–6097.

Polonia, A., Bonatti, E., Camerlenghi, A., Lucchi, R. G., Panieri, G. & Gasperini, L. (2013): Mediterranean megaturbidite triggered by the AD 365 Crete earthquake and tsunami. – Scientific reports **3:** 1285, doi: 10.1038/srep01285.

Quintela, M., Costa, P. J., Fatela, F., Drago, T., Hoska, N., Andrade, C. & Freitas, M. C. (2016): The AD 1755 tsunami deposits onshore and offshore of Algarve (south Portugal): Sediment transport interpretations based on the study of Foraminifera assemblages. – Quaternary International **408:** 123–138.

Reicherter, K., Papanikolaou, I., Roger, J., Mathes-Schmidt, M., Papanikolaou, D., Rössler, S., Grützner, C. & Stamatis, G. (2010): Holocene tsunamigenic sediments and tsunami modeling in the Thermaikos Gulf area (northern Greece). – Zeitschrift für Geomorphologie Supplementary Issues **54** (3): 99–126.

Reilinger, R., McClusky, S., Vernant, P., Lawrence, S., Ergintav, S., Cakmak, R., Ozener, H., Kadirov, F. Guliev, I., Stepanyan, R., Nadariya, M., Hahubia, G., Mahmoud, S., Sakr, K., Ar-Rajehi, A., Paradissis, D., Al-Aydrus, A., Prilepin, M., Guseva, T., Evren, E., Dmitrotsa, A., Filikov, S. V., Gomez, F., Al-Ghazzi, R. & Karam, G. (2006): GPS constraints on continental deformation in the Africa-Arabia-Eurasia continental collisional zone and implications for the dynamics of plate interactions. – Journal of Geophysical Research, Solid Earth **111:** 2–26.

Reimer, P. J., Bard, E., Bayliss, A., Beck, J. W., Blackwell, P. G., Ramsey, C. B., Buck, C. E., Cheng, H., Edwards, R. L., Friedrich, M., Grootes, P. M., Guilderson, T. P., Haflidason, H., Hajdas, I., Hatté, C., Heaton, T. J., Hoffmann, D. L., Hogg, A. G., Hughen, K. A., Kaiser, K. F., Kromer, B., Manning, S. W., Niu, M., Reimer, R. W., Richards, D. A., Scott, E. M., Southon, J. R., Staff, R. A., Turney, C. S. M. & von der Pflicht, J. (2013): Intcal13 and Marine 13 radiocarbon age calibration curves 0–50,000 years cal BP. – Radiocarbon **55** (4): 1869–1887.

Reinhardt, E. G., Patterson, R. T. & Schröder-Adams, C. J. (1994): Geoarchaeology of the ancient harbor site of Caesarea Maritima, Israel: evidence from sedimentology and palaeoecology of benthic foraminifera. – Journal of Foraminiferal Research **24** (1): 37–48.

Richmond, B., Szczuciński, W., Chagué-Goff, C., Goto, K., Sugawara, D., Witter, R., Tappin, D. R., Jaffe, B., Fujino, S., Nishimura, Y. & Goff, J. (2012): Erosion, deposition and landscape change on the Sendai coastal plain, Japan, resulting from the March 11, 2011 Tohoku-oki tsunami. – Sedimentary Geology **282:** 27–39.

Rodríguez-Ramírez, A., Villarías-Robles, J. J. R. Pérez-Asensio, J. N., Santos, A., Morales, J. A., Celestino-Pérez, S., León, A. & Santos-Arévalo, F. J. (2016): Geomorphological record of extreme wave events during Roman times in the Guadalquivir estuary (Gulf of Cadiz, SW Spain): An archaeological and paleogeographical approach. – Geomorphology **261:** 103–118.

Röbke, B. R. & Vött, A. (2017): The Tsunami phenomenon. – Progress in Oceanography **159:** 296–322, doi: 10.1016/j.pocean.2017.09.003.

Rönnfeld, W. (2008): Foraminiferen – Ein Katalog typischer Foraminiferen. – Institut für Geowissenschaften der Universität Tübingen, 146 pp., Tübingen.

Royden, L. H. & Papanikolaou, D. J. (2011): Slab segmentation and late Cenozoic disruption of the Hellenic arc. – Geochemistry, Geophysics, Geosystems **12** (3): 1–24.

Scheffers, A. & Scheffers, S. (2007): Tsunami deposits on the coastline of west Crete (Greece). – Earth and Planetary Science Letters **259** (3): 613–624.

Sdao, F., Parisi, S., Kalisperi, D., Pascale, S., Soupios, P., Lydakis-Simantiris, N. & Kouli, M. (2012): Geochemistry and quality of the groundwater from the karstic and coastal aquifer of Geropotamos River Basin at north-central Crete, Greece. – Environmental Earth Sciences **67** (4): 1145–1153.

Seidel, M., Seidel, E. & Stöckhert, B. (2007): Tectono-sedimentary evolution of lower to middle Miocene half-graben basins related to an extensional detachment fault (western Crete, Greece). – Terra Nova **9:** 39–47.

Shaw, B. (2012): The AD 365 earthquake: Large tsunamigenic earthquakes in the Hellenic Trench. – Active tectonics of the Hellenic subduction zone. – Springer Thesis, 7–28, Springer, Berlin, Heidelberg, doi: 10.1007/978-3-642-20804-1_2.

Shaw, B. & Jackson, J. (2010): Earthquake mechanisms and active tectonics of the Hellenic subduction zone. – Geophysical Journal International **181:** 966–984.

Shaw, B., Ambraseys, N. N., England, P. C., Floyd, M. A., Gorman, G. J., Higham, T. F. G., Jackson, J. A., Nocquet, J.-M., Pain, C. C. & Piggott, M. D. (2008): Eastern Mediterranean tectonics and tsunami hazard inferred from the AD 365 earthquake. – Nature Geoscience **1:** 268–276, doi: 10.1038/ngeo151.

Smedile, A., De Martini, P. M., Pantosti, D., Bellucci, L., Del Carlo, P., Gasperini, L., Pirrotta, C., Polonia, A. & Boschi, E. (2011): Possible tsunami signatures from an integrated study in the Augusta Bay offshore (Eastern Sicily, Italy). – Marine Geology **281:** 1–13.

Soloviev, S. L., Solovieva, O. N., Go, C. N., Kim, K. S. & Shchetnikov, N. A. (2000): Tsunamis in the Mediterranean Sea 2000 B. C. – 2000 A. D. – Springer, 237 pp., Netherlands, Dordrecht.

Soukissian, T., Prospathopoulos, A., Hatzinaki, M. & Kabouridou, M. (2008): Assessment of the wind and wave climate of the Hellenic Seas using 10-year hindcast results. – Open Ocean Engineering Journal **1:** 1–12.

Spratt, T. A. B. (1865): Travels and Researches in Crete. – Harvard University Press, 484 pp., London.

Stiros, S. C. (2001): The AD 365 Crete earthquake and possible seismic clustering during the fourth to sixth centuries AD in the Eastern Mediterranean: a review of historical and archaeological data. – Journal of Structural Geology **23:** 545–562.

Switzer, A. D. & Jones, B. G. (2008): Large-scale washover sedimentation in a freshwater lagoon from the southeast Australian coast: sea-level change, tsunami or exceptionally large storm? – The Holocene **18** (5): 787–803.

Tanaka, H., Tinh, N. X., Umeda, M., Hirao, R., Pradjoko, E., Mano, A. & Udo, K. (2012): Coastal and estuarine morphology changes induced by the 2011 Great East Japan Earthquake Tsunami. – Coastal Engineering Journal **54** (1): 1–25.

Tanaka, H., Kayane, K., Adityawan, M. B., Roh, M. & Farid, M. (2014): Study on the relation of river morphology and tsunami propagation in rivers. – Ocean Dynamics **64** (9): 1319–1332.

Taymaz, T., Jackson, J. & Westaway, R. (1990): Earthquake mechanisms in the Hellenic trench near Crete. – Geophysical Journal International **102:** 695–731.

Tiberti, M. M., Basili, R. & Vannoli, P. (2014): Ups and downs in western Crete (Hellenic subduction zone). – Scientific reports **4:** 1–7.

Tinti, S. (1991): Assessment of tsunami hazard in the Italian seas. – Natural Hazards **4:** 267–283.

Tolkova, E. & Tanaka, H. (2016): Tsunami Bores in Kitakami River. – Pure and Applied Geophysics **173:** 4039, doi: 10.1007/s00024-016-1351-7.

Triantaphyllou, M. V., Koukousioura, O. & Dimiza, M. D. (2009): The presence of the Indo-Pacific symbiont-bearing foraminifer *Amphistegina lobifera* in Greek coastal ecosystems (Aegean Sea, Eastern Mediterranean). – Mediterranean Marine Science **10** (2): 73–85.

Tsoukala, V. K., Chondros, M., Kapelonis, Z. G., Martzikos, N., Lykou, A., Belibassakis, K. & Makropoulos, C. (2016): An integrated wave modelling framework for extreme and rare events for climate change in coastal areas – the case of Rethymno, Crete. – Oceanologia **58** (2): 71–89.

Tsuji, Y., Yanuma, T., Murata, I. & Fujiwara, C. (1991): Tsunami ascending in rivers as an undular bore. – Natural Hazards **4:** 257–266.

Tyuleneva, N., Braun, Y., Katz, T., Suchkov, I. & Goodman-Tchernov, B. (2018): A new chalcolithic-era tsunami event identified in the offshore sedimentary record of Jisr al-Zarka (Israel). – Marine Geology **396:** 67–78.

van Hinsbergen, D. J., Hafkenscheid, E., Spakman, W., Meulenkamp, J. E. &Wortel, R. (2005): Nappe stacking resulting from subduction of oceanic and continental lithosphere below Greece. – Geology **33** (4): 325–328.

Viana-Baptista, M. A., Soares, P. M., Miranda, J. M. & Luis, J. F. (2006): Tsunami propagation along Tagus estuary (Lisbon, Portugal) preliminary results. – Science of Tsunami Hazards **24** (5): 329–338.

Vött, A. & May, S. M. (2009): Auf den Spuren von Tsunamis im östlichen Mittelmeer. – Geographische Rundschau **12:** 42–48.

Vött, A., Brückner, H., May, S. M., Sakellariou, D., Nelle, O., Lang, F., Kapsimalis, V., Jahns, S., Herd, R., Handl, M. & Fountoulis, I. (2009): The Lake Voulkaria (Akarnania, NW Greece) palaeoenvironmental archive – a sediment trap for multiple tsunami impact since the mid-Holocene. – Zeitschrift für Geomorphologie N. F., Supplementary Issue **53** (1): 1– 37.

Vött, A., Lang, F., Brückner, H., Gaki-Papanastassiou, K., Maroukian, H., Papanastassiou, D., Giannikos, A., Hadler, H., Handl, M., Ntageretzis, K., Willershäuuser, T. & Zander, A. (2011a): Sedimentological and geoarchaeological evidence of multiple tsunamigenic imprint on the Bay of Palairos-Pogonia (Akarnania, NW Greece). – Quaternary International **242:** 213–239.

Vött, A., Bareth, G., Brückner, H., Lang, F., Sakellariou, D., Hadler, H., Ntageretzis, K. & Willershäuser,T. (2011b): Olympia's harbour site Pheia (Elis, western Peloponnese, Greece) destroyed by tsunami impact. – Die Erde **142** (3): 259–288.

Vött, A., Hadler, H., Willershäuser, T., Ntageretzis, K., Brückner, H., Warnecke, H., Grootes, P. M., Lang, F., Nelle, O. & Sakellariou, D. (2014): Ancient harbours used as tsunami sediment traps – the case study of Krane (Cefalonia Island, Greece). – In: Ladstätter, S., Pirson, F. & Schmidts, T. (eds.): Häfen und Hafenstädte im östlichen Mittelmeerraum von der Antike bis in byzantinische Zeit. Neue Entdeckungen und aktuelle Forschungsansätze, pp. 743–771. Harbors and Harbor Cities in the Eastern Mediterranean from Antiquity to the Byzantine Period: Recent Discoveries and Current Approaches. – Byzas 19, Veröffentlichungen des Deutschen Archäologischen Instituts Istanbul, Österreichisches Archäologisches Institut Sonderschriften **52** (II), Istanbul.

Vött, A., Fischer, P., Röbke, B. R., Werner, V., Emde, K., Finkler, C., Hadler, H., Handl, M., Ntageretzis, K. & Willershäuser, T. (2015): Holocene fan alluviation and terrace formation by repeated tsunami passage at Epitalio near Olympia (Alpheios River valley, Greece). – Zeitschrift für Geomorphologie N. F., Supplementary Issue **59** (4): 81–123.

Vött, A., Hadler, H., Koster, B., Mathes-Schmidt, M., Röbke, B. R., Willershäuser, T. & Reicherter, K. (2018a): Returning to the facts: Response to the refusal of tsunami traces in the ancient harbour of Lechaion (Gulf of Corinth, Greece) by 'non-catastrophists' – Reaffirmed evidence of harbour destruction by historical earthquakes and tsunamis in AD 69–79 and the 6th cent. AD and a preceding pre-historical event in the early 8th cent. BC. – Zeitschrift für Geomorphologie, doi: 10.1127/zfg/2018/0519.

Vött, A., Bruins, H. J., Gawehn, M., Goodman-Tchernov, B. N., De Martini, P. M., Kelletat, D., Mastronuzzi, G., Reicherter, K., Röbke, B. R., Scheffers, A., Willershäuser, T., Avramidis, P., Bellanova, P., Costa, P. J. M., Finkler, C., Hadler, H., Koster, B., Lario, J., Reinhardt, E., Mathes-Schmidt, M., Ntageretzis, K., Pantosti, D., Papanikolaou, I., Sansò, P., Scicchitano, G., Smedile, A. & Szczuciński, W. (2018b): Publicity waves based on manipulated geoscientific data suggesting climatic trigger for majority of tsunami findings in the Mediterranean – Response to 'Tsunamis in the geological record: Making waves with a cautionary tale from the Mediterranean' by Marriner et al. (2017). – Zeitschrift für Geomorphologie N. F., Supplementary Issue, http://doi.org/10.1127/zfg_suppl/2018/0547.

Werner, V., Baika, K., Fischer, P., Hadler, H., Obrocki, L., Willershäuser, T., Tzigounaki, A., Tsigkou, A., Reicherter, K., Papanikolaou, I., Emde, E., & Vött, A. (2018a): The sedimentary and geomorphological imprint of the AD 365 tsunami on the coasts of southwestern Crete (Greece) – Examples from Sougia and Palaiochora. – Quaternary International **473:** 66–90.

Werner, V., Baika, K., Tzigounaki, A., Reicherter, K., Papanikolaou, I., Emde, K., Fischer, P. & Vött, A. (2018b): Mid-Holocene tectonic geomorphology of northern Crete deduced from a coastal sedimentary archive near Rethymnon and a Late Bronze Age Santorini tsunamite candidate. – Geomorphology, doi: https://doi.org/10.1016/j.geomorph.2018.09.017

Willershäuser, T., Vött, A., Brückner, H., Bareth, G., Nelle, O., Nadeau, M.-J., Hadler, H. & Ntageretzis, K. (2013): Holocene tsunami landfall along the shores of the inner Gulf of Argostoli (Cefalonia Island, Greece). – Zeitschrift für Geomorphologie N. F., Supplementary Issue **57** (4): 105–138.

Willershäuser, T., Vött, A., Hadler, H., Fischer, P., Röbke, B., Ntageretzis, K., Emde, K. & Brückner, H. (2015): Geo-scientific evidence of tsunami impact in the Gulf of Kyparissia (western Peloponnese, Greece). – Zeitschrift für Geomorphologie N. F., Supplementary Issue **59** (4): 43–80.

Addresses of the authors:

Vera Werner*, Kurt Emde, Peter Fischer and Andreas Vött, Institute of Geography, Natural Hazard Research and Geoarchaeology, Johannes Gutenberg-Universität, Johann-Joachim-Becher-Weg 21, 55099 Mainz, Germany

Kalliopi Baika, Aix-Marseille Université, CNRS, CCJ, 5 Rue Château de l'Horloge, 13090 Aix-en-Provence, France and Ephorate of Underwater Antiquities, Hellenic Ministry of Culture, Greece

Anastasia Tzigounaki, Ephorate of Antiquities of Rethymnon, Hellenic Ministry of Culture, Arkadiou 214, Rethymnon, 74 100 Crete, Greece

Klaus Reicherter, Institute of Neotectonics and Natural Hazards, RWTH Aachen University, Lochnerstr. 4–20, 52056 Aachen, Germany

Ioannis Papanikolaou, Mineralogy-Geology Laboratory, Department of Natural Resources Development and Agricultural Engineering, Agricultural University of Athens, 75 Iera Odos Street, 118 55 Athens, Greece

*Corresponding author: v.werner@geo.uni-mainz.de

Manuscript received: 19 December 2018
Manuscript accepted: 14 January 2019